Characterization of the dual functions of *Leishmania* CK1.2 in both the parasite and the macrophage

Daniel MARTEL[1,2], Olivier Leclercq[1,2], Florent Dingli[3], Victor Laigle[3], Damarys Loew[3], Gerald F. SPÄTH[2] and Najma RACHIDI[1,2*].

[1] Institut Pasteur, Université Paris Cité and INSERM U1201, Groupe de signalisation et interactions hôte-parasite, Paris, France

[2] Institut Pasteur, Université de Paris and INSERM U1201, Unité de Parasitologie moléculaire et Signalisation, Paris, France

[3] Laboratoire de Spectrométrie de Masse Protéomique (LSMP), Centre de Recherche, Institut Curie, PSL Research University, Paris, France

Running Title: *The dual function of* Leishmania *CK1.2 in the parasite and its host cell*

*corresponding author: najma.rachidi@pasteur.fr

Keywords: CK1; Interactome; Localisation; Macrophage; *Leishmania*.

Abstract

Leishmania CK1.2 (L-CK1.2) is a serine/threonine protein kinase essential for the survival of the protozoan parasite *Leishmania*, the causative agent of Leishmaniasis. This study investigates the dynamic localization pattern of L-CK1.2 and the broad spectrum of its interacting partners within the parasite. Using proteomic analysis and confocal microscopy, we identified 230 L-CK1.2-associated proteins across the parasite life stages, promastigotes (in the insect vector), and amastigotes, (in the phagolysosomes of host macrophages). This analysis revealed the ubiquitous presence of L-CK1.2 in various cellular structures, including the cytoskeleton, basal body, and flagellum. Using an *in vitro* system, sixty-four host L-CK1.2-associated proteins, involved in critical host biological processes such as immune response, apoptosis, and purine biosynthesis, were shown to interact with L-CK1.2. These processes are known to be regulated by *Leishmania* during infection. The study highlights the dual function of L-CK1.2, in the parasite (cis) and within the host cell (trans), positioning this kinase as a key player in host-pathogen interactions. This work provides a comprehensive map of L-CK1.2 interactions and suggest its potential importance in regulating intracellular *Leishmania* survival, providing potential therapeutic targets for Leishmaniasis. Furthermore, given the evolutionary conservation of CK1.2 across other parasitic organisms, our findings may have broader implications for understanding and managing parasitic infections.

Introduction

CK1 family members are serine/threonine protein kinases ubiquitously expressed in eukaryotic organisms (1). They are involved in a wide range of important cellular processes, such as membrane trafficking or vesicular transport from yeast to humans (1). Due to its broad spectrum of action, CK1 activity and expression are tightly regulated by several mechanisms, including phosphorylation and subcellular sequestration (1). Indeed, members of the CK1 family are associated with many subcellular structures and organelles through interactions with specific partners ranging from circadian clock to cytoskeletal elements, (2-7), reflecting the strong interconnection of CK1 localisation and its functions.

44 Defects in regulation, localisation or the introduction of mutations in the CK1 coding sequence are often
45 associated with important diseases like cancer or neurodegenerative diseases (8) (9) (10). Regulation of
46 CK1 pathways has also been linked to infectious diseases. For instance, inhibiting host CK1 suppresses
47 yellow fever virus replication (11), highlighting the crucial role of CK1 in host-pathogen interactions.
48 The protozoan parasite *Leishmania* is the causative agent of Leishmaniasis, a potentially life-threatening
49 disease with at least three distinct clinical forms, cutaneous, mucocutaneous and the fatal visceral
50 leishmaniasis. *Leishmania* has two developmental stages, an extracellular promastigote stage that
51 proliferates inside the insect vector, and an intracellular amastigote stage that develops and multiplies
52 inside the phagolysosomes of macrophages. The *Leishmania* genome encodes for six CK1 paralogs (12),
53 of which only CK1.2 and CK1.4 are secreted by the parasite and were shown to be essential for parasite
54 survival (13, 14). Several lines of evidence suggest that CK1.2 is released within the host cell as free
55 protein or via extracellular vesicles (15-17). The adaptation of L-CK1.2 to two distinct cellular
56 environments, driven by the high conservation of its protein sequence in *Leishmania* spp. and strong
57 identity to its human orthologs, suggests that this protein has been shaped by selective pressures acting
58 both on its functions within the host cell (12, 18). Indeed, our previous study identified potential
59 substrates of L-CK1.2 in the macrophage, indicating its ability to regulate multiple host biological
60 processes, such as 'viral & symbiotic interaction', 'actin cytoskeleton organization' and 'apoptosis'
61 (19). This potentially dual functions, in *cis* in the parasite and in *trans* in the host macrophage (12, 18,
62 19), suggest *Leishmania* CK1.2 as a key player in host-pathogen interactions. Despite its importance in
63 parasite biology and infection, the functions of L-CK1.2 remain poorly understood, beyond its known
64 interactions with and phosphorylation of heat shock proteins within the parasite, and its ability to
65 phosphorylate host targets such as IFNAR1, IFNAR2 (interferon-α/β receptors)(12, 13, 19-22). The
66 essential nature of this kinase and its involvement in most cellular functions present major challenges
67 for functional analysis using genetic approaches. To overcome these limitations and gain insights into
68 the cis and trans functions of L-CK1.2, we chose a complementary approach determining and comparing
69 its interactomes in both the parasite and the host cell. Our proteomic analysis unveils a repertoire of 230
70 interacting partners for L-CK1.2 across both amastigote and promastigote life stages of the parasite,
71 with Gene Ontology enrichment analyses indicating its ubiquitous nature and multifaceted localization

72 within various organelles. Applying confocal microscopy, we confirmed the localization of L-CK1.2 at
73 these key subcellular sites, including the cytoskeleton, basal body, and flagellum. We used an *in vitro*
74 approach to further identify 64 host proteins interacting with L-CK1.2, which again are implicated in a
75 wide range of biological processes such as immune response, apoptosis and purine biosynthetic process.
76 These biological processes are also modulated during *Leishmania* infection, strongly suggesting the
77 involvement of L-CK1.2 in subverting host cell signalling. Our results suggest that certain pathways
78 identified in the parasite as potential targets of L-CK1.2 are similarly found in the host. Collectively,
79 our data provide additional evidence for the essential role of L-CK1.2, as a central component of the
80 trans-signalling network between *Leishmania* and the macrophage. This dual biological function opens
81 exciting avenues for future research on the co-evolution of parasite and macrophage biology, and the
82 discovery of host-directed therapeutic interventions.
83

84 # Materials and Methods

85 ## *Leishmania* cell lines

86 All the parasite cell lines used in this study were derived from *L. donovani* axenic 1S2D
87 (MHOM/SD/62/1S-CL2D) clone *Ld*Bob, obtained from Steve Beverley, Washington University School
88 of Medicine, St. Louis, MO. Promastigotes were cultured and differentiated into axenic amastigotes as
89 described previously (23). Parasites cell lines were grown in media with 30 µg/mL hygromycin B
90 (ThermoFisher Scientific Cat# 10687010) to maintain the pLEXSY-CK1.2-V5 or the empty pLEXSY
91 plasmids. The transgenic *L. donovani* cell lines containing either the pLEXSY or pLEXSY-CK1.2-V5-
92 HIS_6 (pLEXSY-CK1.2-V5) vectors, corresponding to the mock or expressing *Leishmania major* CK1.2
93 tagged with V5 and HIS_6, respectively, were described previously (18). L-CK1.2-V5 in this strain was
94 shown to be active, functional, able to rescue a decrease in the activity of endogenous CK1.2 and its
95 ectopic expression did not alter the parasite phenotypes.

96 **Immunofluorescence**

97 To confirm the localisation of CK1.2 inferred from the interactome dataset, we used the *Leishmania*
98 *donovani* mock and CK1.2-V5 parasites (see Mat & Met and (18)). Although, CK1.2-V5 is expressed
99 ectopically, its abundant is twice as less as the endogenous CK1.2, precluding the risk of localisation
100 artefact due to overexpression. Logarithmic phase promastigotes or axenic amastigotes (48h after shift
101 at 37°C and pH5.5) were resuspended at $2x10^6$ parasites per mL in Dulbecco's Phosphate Buffer Saline
102 (DPBS) (Gibco) from at least three biological replicates, and 500 µL were added to poly-L-lysine-coated
103 coverslips placed in a 24-well plate. Plates were centrifuged 10 min at 1200 g at room temperature to
104 settle parasites onto the coverslips. For fixation alone, cells were washed three times with DPBS and
105 fixed in 4% paraformaldehyde (PFA) in DPBS for 15 min at room temperature. For cytoskeleton
106 preparation, the protocol was adapted from (24). Briefly, cells were washed three times with DPBS,
107 treated with 0.125% Nonidet 40 (Fluka BioChemika Cat# 74385) in PIPES buffer (100 mM piperazine-
108 N,N-bis(2-ethanesulfonic acid) (PIPES) pH6.8, 1 mM $MgCl_2$) for 2 minutes at room temperature and
109 washed twice for 5 minutes in PIPES buffer. Cells were fixed in 4% PFA in DPBS for 15 min at room
110 temperature. After PFA fixation, cells were washed three times in DPBS, neutralised 10 min with NH_4Cl
111 (50 mM in DPBS), and washed again three times in DPBS. For the immuno-labelling of PFA-fixed cells
112 or cytoskeleton preparations, the samples were blocked with 10% filtered heat-inactivated fetal calf
113 serum (FCS) containing 0.5 $mg.mL^{-1}$ saponin in DPBS for 30 min at room temperature and then washed
114 for 5 min in DPBS. The cells were then incubated with primary antibodies diluted in DPBS with 0.5%
115 Bovine Serum Albumin (BSA) and 0.5 $mg.mL^{-1}$ saponin for 1h at room temperature. Three washes of
116 10 min were performed and the secondary antibody diluted in DPBS with 0.5% BSA and 0.5 $mg.mL^{-1}$
117 saponin was added. After one hour incubation at room temperature in the dark, cells were washed twice
118 for 10 min in DPBS with 0.5% BSA and 0.5 $mg.mL^{-1}$ saponin, and then twice in DPBS. Parasites were
119 incubated with 5 $\mu g.mL^{-1}$ Hoechst 33342 in DPBS for 8 min in the dark, washed twice with DPBS, one
120 time with distilled water, air-dried, then mounted with slides using SlowFade Gold Antifade Mountant
121 (ThermoFisher Scientific Cat# S36937). For methanol fixation, logarithmic phase promastigotes were
122 washed twice in DPBS and resuspended at $2x10^7$ parasites per mL. 10^6 parasites were spread onto poly-
123 L-lysine coated slides and allowed to settle for 30 min in a humid chamber. Parasites were then fixed in

124 methanol at -20°C for 3 minutes and rehydrated for 10 min in DPBS at room temperature. For immuno-
125 labelling of methanol-fixed parasites, samples were blocked with 10% filtered heat-inactivated FCS in
126 DPBS for 15 min at room temperature and washed for 5 min in DPBS. Then the cells were treated
127 similarly as those fixed by PFA. The antibodies used were: mouse IgG2a anti-V5 tag monoclonal
128 antibody (Thermo Fisher Scientific Cat# R960-25, RRID:AB_2556564) diluted at 1/200 (in PFA and
129 methanol fixed parasites) or at 1/300 (in cytoskeleton preparations); rabbit anti-V5 tag polyclonal
130 antibody (Abcam Cat# ab9116, RRID:AB_307024) diluted at 1/400; rabbit anti-LdCentrin polyclonal
131 antibody (kind gift from Hira L. Nakhasi) diluted at 1/2000 (25); mouse IgG1 anti-IFT172 monoclonal
132 antibody diluted at 1/200 (26); mouse anti-PFR2 L8C4 clone antibody diluted at 1/10 (27); mouse L1C6
133 anti-TbNucleolus monoclonal antibody diluted at 1/100 (kind gift from Keith Gull (28)); mouse IgG1
134 anti-α-tubulin monoclonal DM1A antibody (Sigma-Aldrich Cat# T9026, RRID:AB_477593) diluted at
135 1/400; chicken anti-Hsp70 and chicken anti-Hsp90 antibodies diluted at 1/200 (29). IgG subclass-
136 specific secondary antibodies coupled to different fluorochromes were used for double labelling: anti-
137 mouse IgG (H+L) coupled to AlexaFluor488 (1/200 (PFA- or methanol-fixed parasites)) or 1/300
138 (cytoskeleton preparations), Thermo Fisher Scientific Cat# A-21202, RRID:AB_141607)); anti-mouse
139 IgG2a coupled to Cy3 (1/600; Jackson ImmunoResearch Labs Cat# 115-165-206, RRID:AB_2338695);
140 anti-mouse IgG1 coupled to AlexaFluor647 (1/600; Thermo Fisher Scientific Cat# A-21240,
141 RRID:AB_2535809); anti-rabbit IgG (H+L) coupled to AlexaFluor488 (1/400; Thermo Fisher
142 Scientific Cat# A-21206, RRID:AB_2535792); anti-mouse IgG (H+L) coupled to AlexaFluor594
143 (1/200; Thermo Fisher Scientific Cat# A-21203, RRID:AB_2535789); anti-mouse IgG2a coupled to
144 AlexaFluor488 (1/300; Thermo Fisher Scientific Cat# A-21131, RRID:AB_2535771); anti-mouse IgG1
145 coupled to AlexaFluor594 (1/300; Thermo Fisher Scientific Cat# A-21125, RRID:AB_2535767); anti-
146 chicken IgY coupled to AlexaFluor594 (1/200; Jackson ImmunoResearch Labs Cat# 703-586-155,
147 RRID:AB_2340378) and anti-rabbit IgG (H+L) coupled to AlexaFluor594 (1/400; Thermo Fisher
148 Scientific Cat# A-21207, RRID:AB_141637).

149 **Confocal microscopy**

150 Images were visualised using a Leica SP5 HyD resonant scanner Matrix screener inverted microscope
151 equipped with a HCX PL APO CS 63x, 1.4 NA oil objective (Leica, Wetzlar, Germany). Triple or
152 quadruple immunofluorescence was imaged with Leica Application Suite AF software (LAS AF; Leica
153 Application Suite X, RRID:SCR_013673) after excitation of the Hoechst 33342 dye with a diode at a
154 wavelength of 405 nm (452/75 Emission Filter), excitation of the AlexaFluor488 with an argon laser at
155 a wavelength of 488 nm (525/50 Emission Filter), excitation of AlexaFluor594 with a diode DPSS at a
156 wavelength of 561 nm (634/77 Emission Filter), excitation of Cy3 with a diode DPSS at a wavelength
157 of 561 nm (595/49 Emission Filter), and excitation of AlexaFluor647 with a helium-neon laser at a
158 wavelength of 633 nm (706/107 Emission Filter). Images were scanned sequentially to minimise cross
159 excitation between channels and each line was scanned twice and averaged to increase the signal-to-
160 noise ratio. The pinhole aperture was set to 1 airy. Images were acquired with 8x zoom at a resolution
161 of 1024×1024. Z-stacks were acquired at 0.082 µm intervals, deconvolved and rendered using either
162 Fiji (RRID:SCR_002285) or Icy (RRID:SCR_010587) software (30) (http://icy.bioimageanalysis.org/).

163 **Deconvolution of z-stacks and chromatic aberration correction**

164 All confocal images were processed and analysed by using the Huygens Professional software version
165 19.04 (Scientific Volume Imaging, Huygens Software, RRID:SCR_014237). Deconvolution of confocal
166 z-stacks was optimised using the following settings: automatic estimation of the average background
167 with the mode "Lowest" and area radius = 0.7, deconvolution algorithm CMLE, maximum number of
168 iterations = 40, signal to noise ratio (SNR) = 20, quality change threshold = 0.05, iteration mode =
169 optimised, brick layout = automatic. Theoretical point spread function (PSF) values were estimated for
170 each *z*-stack. All deconvolved images were corrected for chromatic shifts and for rotational differences
171 between different channels using the Chromatic Aberration Corrector (CAC) from Huygens
172 Professional software (Scientific Volume Imaging, Huygens Software, RRID:SCR_014237). To
173 calibrate the image corrections, multifluorescent 0.2 µm TetraSpeck microspheres (ThermoFisher
174 Scientific Cat#T7280) mounted on SlowFade Gold Antifade mountant (ThermoFisher Scientific Cat#
175 S36937) were imaged with identical acquisition parameters. Images were deconvolved similarly and

176 were used to perform the chromatic aberration estimations with the cross-correlation method in CAC
177 software. Corrections were saved as templates and applied for correction of the similarly acquired and
178 deconvolved images in CAC.

179 **Co-localisation analysis of confocal images**

180 Co-localisation analysis was performed with the Co-localisation Analyzer plug-in of the Huygens
181 Professional software (Scientific Volume Imaging, Huygens Software, RRID:SCR_014237, v19.04).
182 Processed cross-section images (deconvolved and corrected for chromatic aberrations) of the parasites
183 were opened with this plug-in and Pearson correlation coefficients (PCC) were calculated for each
184 parasite to quantify co-localisation. A PCC above 0.5 indicates co-localisation. Specific areas of the
185 parasite were cropped from the whole image (basal body area, flagella pocket area, mitotic spindle and
186 reduced mitotic spindle areas, flagellar pocket neck area and flagellar tip area) with the "crop" tool of
187 the Huygens Professional software. Criteria to crop specific structures from the images were: (1) basal
188 bodies - a region containing one or two dots representing the basal bodies in the channel CEN and
189 excluding most of the flagellar pocket and flagellar pocket neck; (2) flagellar pocket area – a region
190 stained with CK1.2 and CEN but excluding the basal bodies dots and the flagellum; (3) mitotic spindle
191 – the entire Hoechst-unstained nucleus region in mitotic cells, containing the mitotic spindle in the TUB
192 channel; (4) reduced mitotic spindle areas – only the regions containing the TUB staining in the mitotic
193 nuclei, since CK1.2 is present in Hoechst-unstained regions where TUB staining is not visible, co-
194 localisation of the entire Hoechst-unstained region is biased by a strong staining with CK1.2. We
195 decided to crop further to analyse the colocalisation of CK1.2 and TUB in the mitotic spindle stained
196 by TUB; (5) flagellar pocket neck – a region at the junction of the flagellum and the parasite body,
197 excluding most of the flagellar pocket and basal bodies CK1.2 staining; and (6) flagellar tip – region at
198 the tip of the flagellum, containing only a fraction of the rest of the flagellum. Rationale: since CK1.2
199 is present in Hoechst-unstained regions where TUB staining is not visible, co-localisation of the entire
200 Hoechst-unstained region is biased by a strong staining with CK1.2. We decided to crop further to
201 analyse the colocalisation of CK1.2 and TUB in the mitotic spindle stained by TUB. For the analysis of
202 the colocalisation of CK1.2 and TUB in the mitotic spindle stained by TUB, we cropped further to

203 restrict to the mitotic spindle as the co-localisation of the entire Hoechst-unstained region was biased by
204 a strong staining with CK1.2. Pearson coefficients were calculated for these images. Pearson coefficients
205 of the co-localisation in the basal body and flagellar pocket areas of (i) CK1.2-V5 with Centrin (CEN),
206 IFT172, and DNA (Hoechst 33342, H); or (i) CEN with IFT172, from 14 images were plotted in
207 scattered dot plots with the mean and standard deviation using GraphPad Prism 8.1.1 (GraphPad
208 Software, GraphPad Prism, RRID:SCR_002798). Pearson coefficients of the co-localisation of CK1.2-
209 V5 with tubulin in the mitotic spindle and reduced mitotic spindle areas from seven images were plotted
210 similarly. Pearson coefficients of the co-localisation of CK1.2-V5 with Hsp90 from seven images and
211 with Hsp70 from ten images were also plotted similarly.

212 **Epifluorescence microscopy and automated parasite detection**

213 Images were visualised using a Zeiss upright widefield microscope equipped with Apotome2 grids and
214 a Pln-Apo 63x, 1.4 NA oil objective (Zeiss). Light source used was a Mercury Lamp HXP 120, and
215 following filters were used: DAPI (Excitation G365; dichroic FT 395; emission BP 420-470), FITC-
216 A488-GFP (Excitation BP 455-495; dichroic FT 500; emission BP 505-555) and A594-TexasRed-
217 mCherry-HcRed-mRFP (Excitation BP 542-582; dichroic FT 593; emission BP 604-644). Images were
218 captured on an Axiocam MRm camera using ZEN Blue software. For comparison of different cell lines,
219 identical parameters of acquisition were applied on all samples.

220 **Protein extraction, SDS-PAGE and Western blot analysis**

221 Logarithmic phase promastigotes were washed in DPBS and protein extraction was performed as
222 described previously (23). Ten micrograms of total protein were separated by SDS-PAGE, and
223 transferred onto polyvinylidene difluoride (PVDF) membranes (Pierce). Membranes were blocked with
224 5% BSA in DPBS supplemented with 0.25% Tween20 (PBST) and incubated over night at 4°C with
225 primary antibody mouse IgG2a anti-V5 tag monoclonal antibody (1/1000; Thermo Fisher Scientific
226 Cat# R960-25, RRID:AB_2556564) in 2,5% BSA in PBST. Membranes were then washed in PBST and
227 incubated with secondary antibody anti-mouse IgG (H+L) coupled to horseradish peroxidase (1/20000;
228 ThermoFisher Scientific Cat# 32230, RRID:AB_1965958). Proteins were revealed by SuperSignal™
229 West Pico Chemiluminescent Substrate (ThermoFisher Scientific Cat# 34580) using the PXi image

230 analysis system (Syngene) at various exposure times. Membranes were then stained with Bio-Safe
231 Coomassie (Bio-Rad Cat #1610786) to serve as loading controls.

232 **Recombinant expression, purification of CK1.2-V5-His$_6$ and protein kinase assay**

233 *Escherichia coli* Rosetta (DE3) pLysS Competent Cells (Merck Cat# 70956) containing pBAD-thio-
234 topo-L-CK1.2-V5-His$_6$ and pBADthio-V5-His6 (control thioredoxin) were grown at 37°C and induced
235 with arabinose (0,02% final) for 4h at room temperature (18). Cells were harvested by centrifugation at
236 10,000 g for 10 min at 4°C and the recombinant proteins were purified as described previously (18)
237 (31). The eluates were supplemented with 15% glycerol and stored at −80°C.

238 **Production of macrophage extracts**

239 Bone marrow derived macrophages (BMDM) were obtained from BALB/c ByJRj mice (32).
240 Macrophages were lysed with RIPA buffer (150 mM NaCl, 1% Triton X-100, 20 mM Tris HCl [pH
241 7.4], 1% NP-40, 1 mM EDTA) supplemented with complete protease inhibitor cocktail (Roche Applied
242 Science, IN) and with 1 mM sodium orthovanadate and 1 mM PMSF. Macrophage lysates were then
243 vortexed and, after sonication, clarified by centrifugation.

244 **Immuno-precipitation**

245 *Leishmania IP*

246 *L. donovani* logarithmic phase promastigotes or axenic amastigotes (48h post differentiation) containing
247 either pLEXSY (mock) or pLEXSY-CK1.2-V5-His6 (expressing CK1.2-V5-His6) were collected and
248 total protein were extracted, as described previously (23). Six (promastigotes) or twelve milligrams
249 (axenic amastigotes) of total proteins were used at 2 mg/mL concentration in RIPA lysis buffer for the
250 immuno-precipitation. The lysates were pre-cleared for 30 min with 1.5 mg of fresh magnetic beads
251 coupled to protein G (ThermoFisher Scientific Cat# 10003D), washed with DPBS-tween buffer (DPBS
252 with 0.02% Tween-20, adjusted at pH 7.4) and mixed with cross-linked anti-V5-coupled magnetic beads
253 according to the manufacturer protocol. After incubation with pre-cleared lysates, beads were washed
254 then the bound proteins were eluted with the glycine elution buffer for the PRO condition and with

255 glycine elution buffer followed by the NuPAGE loading buffer (invitrogen) and heating at 95°C for Ax
256 AMA condition. Elutions were kept at -80°C before mass spectrometry analysis.
257 *Host IP*
258 The rL-CK1.2-V5, the control thioredoxin and the empty vector were incubated overnight with 142 µg
259 BMDM protein lysates. After preclearing, the samples were incubated with magnetic beads coupled to
260 protein G and cross-linked to anti-V5 antibody. Following washing, the immuno-precipitated proteins
261 were eluted first with glycine elution buffer (elution 1 and 2) then with one elution of NuPAGE loading
262 buffer (elution 3). Elutions 1 and 3 were used for MS analysis and proteins from elution 2 were separated
263 on SDS-PAGE and stained with SYPRO Ruby to assess the IP (Figure 5A).

264 **Size exclusion chromatography**

265 Parasites containing either pLEXSY_HYG_V5_CK1.2 were harvested from logarithmic-phase cultures
266 by centrifugation at 1,600 × g for 10 min and washed three times in D-PBS without $CaCl_2$ and $MgCl_2$
267 (Gibco). Cells were resuspended either in 1X RIPA lysis buffer (Cell Signaling Technology) containing
268 1 mM Phenylmethylsulfonyl fluoride, 50 U/ml Benzonase nuclease, Purity > 90% (VWR) and protease
269 inhibitors (cOmplete Mini, EDTA-free Protease Inhibitor Cocktail Tablets; Roche). Cells suspensions
270 were incubated on ice for 45 min, disrupted by sonication for 5 min (20s pulse, 20s off) in ice and
271 clarified by centrifugation at 12,000 g for 10 min at 4°C. Total protein extracts were quantified using
272 RC DC Protein Assay Kit II (Bio-Rad) then used immediately. SEC fractionations were performed at
273 4°C on Superose 6 increase 10/300 GL column (Cytiva) using a ÄKTApurifier FPLC system (GE
274 Healthcare) (P-900 pumps; INV-907 valve; M-925 mixing valves; FR-902 flow Restrictor; FRC-950
275 fraction collector; UV-900 detector; CU-950 controller) piloted by UNICORN 5.10 software (GE
276 Healthcare). Column was equilibrated with 2 column volumes (CV) of elution buffer (50 mM sodium
277 phosphate; 150 mM NaCl; pH 7.2) at a flow rate of 0.35 ml/min. Then 6.9 milligrams of total protein
278 extract were load in 500 µl sample loop, injected onto the column, and eluted with 1 CV of elution
279 buffer at a flow rate of 0.35 ml/min. Eluted proteins were collected in 96 fractions of 200 µl. Fifteen
280 microliters of each fraction were separated on a Novex NuPAGE 4 to 12% bis-Tris gel (ThermoFischer
281 scientific) followed by Western blotting. Blots were probed with an anti-V5 antibody and an anti-mouse

282 HRP-conjugated antibody. Signals were revealed using SuperSignal West Pico kit (Pierce), monitored
283 with ChemiDoc imager (Bio-Rad) and quantified using Image Lab Software (Bio-Rad).

284 **Mass spectrometry analysis**

285 MS analysis of the samples was done at the "Laboratoire de Spectrométrie de Masse Protéomique
286 (LSMP)" platform at Institut Curie in Paris.

287 *Leishmania IP*

288 Proteins were run on SDS–PAGE gels (Invitrogen) without separation just as a clean-up step and stained
289 with colloidal blue staining (LabSafe GEL Blue™ G Biosciences). Gel slices were excised, and proteins
290 were reduced with 10 mM DTT prior to alkylation with 55 mM iodoacetamide. In-gel digestion was
291 performed using trypsin/Lys-C (Promega) overnight in 25 mM NH4HCO3 at 30 °C. Peptides were then
292 extracted using 60/35/5 MeCN/H2O/HCOOH and vacuum concentrated to dryness. Samples were
293 separated by chromatography using an RSLCnano system (Ultimate 3000, Thermo Scientific) coupled
294 to an Orbitrap Fusion mass spectrometer (Q-OT-qIT, Thermo Fisher Scientific). We acquired Survey
295 MS scans in the Orbitrap with the resolution set to a value of 120,000 and a 4×10^5 ion count target.
296 Each scan was recalibrated in real time by co-injecting an internal standard from ambient air into the C-
297 trap. Tandem MS was performed by isolation at 1.6 Th with the quadrupole, HCD fragmentation with
298 normalized collision energy of 35, and rapid scan MS analysis in the ion trap. The MS2 ion count target
299 was set to 10^4 and the max injection time was 100 ms. Only those precursors with charge state 2–7 were
300 sampled for MS2. The dynamic exclusion duration was set to 60s with a 10 ppm tolerance around the
301 selected precursor and its isotopes. The instrument was run in top speed mode with 3 sec cycles.

302 For identification, the data were searched against the Ld1S2D database
303 (https://www.ncbi.nlm.nih.gov/bioproject/PRJNA396645, GCA_002243465.1) using Sequest HT
304 through Proteome Discoverer (version 2.4). Enzyme specificity was set to trypsin and a maximum of
305 two missed cleavages was allowed. Oxidized methionine and N-terminal acetylation were set as variable
306 modifications and carbamidomethyl cysteine as fixed modification. The mass tolerances in MS and
307 MS/MS were set to 10 ppm and 0.6 Da, respectively. The resulting files were further processed using
308 myProMS v3.9.3 (https://github.com/bioinfo-pf-curie/myproms, (33)). False-discovery rate (FDR) was

309 calculated using Percolator (34) and was set to 1% at the peptide level for the whole study. Label-free
310 quantification was performed using peptide extracted ion chromatograms (XICs), re-extracted within
311 conditions, and computed with MassChroQ v.2.2.21 (35). For protein quantification, XICs from
312 proteotypic peptides shared between compared conditions (TopN matching) with missed cleavages were
313 used. Median and scale normalization at peptide level was applied on the total signal to correct the XICs
314 for each biological replicate (N=3 in both conditions). To estimate the significance of the change in
315 protein abundance, a linear model (adjusted on peptides and biological replicates) was performed, and
316 p-values were adjusted using the Benjamini–Hochberg FDR procedure. Proteins with at least two
317 distinct peptides in two replicates of a same state, 2-fold enrichment and an adjusted p-value ≤ 0.05 were
318 considered significantly enriched in sample comparisons. Proteins unique to a condition were also
319 considered if they matched the peptides criteria. The mass spectrometry proteomics raw data have been
320 deposited to the ProteomeXchange Consortium via the PRIDE (36) partner repository with the dataset
321 identifier pxd033809.

322 *Host IP*

323 The elutions 1 and 3 were also run on SDS-PAGE without separation and only one gel slice containing
324 the entire elution fraction was excised and used for nanoscale liquid chromatography coupled to tandem
325 mass spectrometry (nanoLC-MS/MS) as described in the paragraph *Leishmania IP*. For protein
326 identification, the data were searched against the databases containing SwissProt Mus Musculus (16745
327 sequences), contaminants and Uniprot *L. donovani* CK1.2 by using Sequest HT from Proteome
328 Discoverer (version 2.4 or 2.1). The mass spectrometry proteomics raw data have been deposited to the
329 ProteomeXchange Consortium via the PRIDE (36) partner repository with the dataset identifier: Project
330 accession: PXD064006.

331 **Bioinformatics**

332 The gene ontology analyses were performed with PANTHER (http://www.pantherdb.org/) (37) using
333 *L. major* orthologs as input, or manually annotated using TriTrypDB (https://tritrypdb.org/tritrypdb/app)
334 (38). STRING database, used to visualize protein complexes among the L-CKAP and L-CKAPhost,
335 were merged to the interaction networks of L-CKAP*host* using Cytoscape software (version 3.7.1,

336 https://string-db.org/) (39). The localisation of *T. brucei* proteins was determined using TrypTag website
337 (http://tryptag.org/) (40). The localisation of *Leishmania mexicana* proteins was determined using
338 LeishTag (https://www.leishtag.org/). For motif determination, we used SMART (http://smart.embl-
339 heidelberg.de/). The dataset was analysed for protein-protein interactions and visualized using the
340 STRING plugin (string, https://string-db.org/(41)) of the Cytoscape software package (version 3.8.2,
341 https://cytoscape.org/(42)). Each node represents a substrate, and each edge represents a protein-protein
342 interaction. The text was improved using ChatGPT 3.5 with the prompt, rewrite or improve (version
343 3.5, https://openai.com/chatgpt).

344 Quantification and statistical analysis

345 Statistical analyses were performed with GraphPad Prism 8.1.1 (GraphPad Software, GraphPad Prism,
346 RRID:SCR_002798) using unpaired t test (parametric test). Graphs were drawn using the same
347 software. All errors correspond to the 95% confidence interval. Statistically significant differences are
348 indicated with three ($p<0.01$), four ($p<0.001$) or five asterisks ($p<0.0001$). The number of samples
349 analysed for each experiment is indicated in figure legends.

350 Resource table

REAGENT or RESOURCE	SOURCE	IDENTIFIER
Antibodies		
Anti-V5 tag IgG2a mouse monoclonal	Thermo Fisher Scientific	Cat# R960-25, RRID:AB_2556564
Anti-Centrin from *L. donovani* rabbit polyclonal	(25)	N/A
Anti-IFT172 from *T. brucei* IgG1 mouse monoclonal	(26)	N/A
Anti-V5 tag IgG rabbit polyclonal	Abcam	Cat# ab9116, RRID:AB_307024

Anti-PFR2 from *T. brucei* mouse polyclonal (L8C4)	(27)	N/A
Anti-nucleolus IgG from *T. brucei* mouse monoclonal (L1C6)	Keith Gull, University of Oxford, UK	N/A
Anti-alpha-tubulin IgG1 mouse monoclonal DM1A	Sigma-Aldrich	Cat# T9026, RRID:AB_477593
Anti-mouse IgG (H+L) coupled to AlexaFluor488	Thermo Fisher Scientific	Cat# A-21202, RRID:AB_141607
Anti-mouse IgG2a coupled to Cy3	Jackson ImmunoResearch Labs	Cat# 115-165-206, RRID:AB_2338695
Anti-mouse IgG1 coupled to AlexaFluor647	Thermo Fisher Scientific	Cat# A-21240, RRID:AB_2535809
Anti-rabbit IgG (H+L) coupled to AlexaFluor488	Thermo Fisher Scientific	Cat# A-21206, RRID:AB_2535792
Anti-mouse IgG (H+L) coupled to AlexaFluor594	Thermo Fisher Scientific	Cat# A-21203, RRID:AB_2535789
Anti-mouse IgG2a coupled to AlexaFluor488	Thermo Fisher Scientific	Cat# A-21131, RRID:AB_2535771
Anti-mouse IgG1 coupled to AlexaFluor594	Thermo Fisher Scientific	Cat# A-21125, RRID:AB_2535767
Anti-chicken IgY coupled to AlexaFluor594	Jackson ImmunoResearch Labs	Cat# 703-586-155, RRID:AB_2340378
Anti-rabbit IgG (H+L) coupled to AlexaFluor594	Thermo Fisher Scientific	Cat# A-21207, RRID:AB_141637
Anti-mouse IgG (H+L) coupled to horseradish peroxidase	Thermo Fisher Scientific	Cat# 32230, RRID:AB_1965958
Bacterial Strains		

Escherichia coli Rosetta (DE3) pLysS Competent Cells	Merck	Cat# 70956
Experimental Models: Organisms/Cell lines		
*Ld*Bob cells with pLEXSY vector (mock)	(18)	N/A
*Ld*Bob cells with pLEXSY-CK1.2-V5-His_6 vector, expressing *Lma*CK1.2-V5-His_6	(18)	N/A
Chemicals, Peptides, and Recombinant Proteins		
Nonidet P40 (NP40)	Fluka BioChemika	Cat# 74385
Ammonium Chloride (NH_4Cl)	VWR Chemicals	Cat# 21235.297
Carbobenzoxy-Leu-Leuleucinal (MG132)	Sigma-Aldrich	Cat# M7449
SlowFade Gold Anti-Fade	ThermoFisher Scientific	Cat# S36937
Recombinant thio-*Lma*CK1.2-V5-His_6	(18)	N/A
Recombinant MBP	Sigma-Aldrich	Cat# M1891
Recombinant DNA		
Plasmid: pLEXSY-hyg2 (HygR)	Jena Bioscience	Cat# EGE-232
Plasmid: pLEXSY-CK1.2-V5-His_6 (HygR)	(18)	N/A
Software and Algorithms		
Icy	Icy	RRID:SCR_010587
GraphPad Prism	GraphPad	RRID:SCR_002798
CytExpert Software	Beckman Coulter	RRID:SCR_017217, v2.2.0.97
Fiji	Fiji	RRID:SCR_002285
Huygens Professional	Scientific Volume Imaging	RRID:SCR_014237

Leica Application Suite AF (LAS AF)	Leica	RRID:SCR_013673

351

352

353 ## Results

354 ### *Leishmania* CK1.2 displays a pleiotropic localisation and interacts with numerous
355 proteins in promastigotes and in axenic amastigotes

356 To determine L-CK1.2 localisation, we used the transgenic *L. donovani* Bob (*Ld*Bob) parasites carrying
357 either the empty pLEXSY vector (referred to as 'mock') or pLEXSY-CK1.2-V5-His_6 (referred to as
358 'CK1.2-V5'), (18), previously characterised and functionally validated (18). Both strains were fixed
359 with paraformaldehyde (PFA). L-CK1.2 was detected as intense punctate staining in the cytoplasm and
360 the flagellum of PFA-fixed promastigotes expressing L-CK1.2-V5 (Figure 1Aa) but not in the
361 corresponding mock control, which only showed weak background fluorescence (Figure 1Ab). The sum
362 of the fluorescence intensity in the body of CK1.2-V5 promastigotes was significantly higher than that
363 of the mock parasites with a p-value below 0.0001 (Figure S1A), indicating that this punctate staining
364 is specific to CK1.2-V5. Similar localisations were also observed for axenic amastigotes (Figure 1Ac).
365 This pleiotropic localization aligns with the diverse functions attributed to this protein kinase family.
366 However, in the absence of a signal peptide for specific targeting, CK1 family members may primarily
367 depend on protein-protein interactions for their localization (17).

368 To assess whether L-CK1.2 engages in protein-protein interactions in *Leishmania* promastigotes, we
369 subjected V5-tagged L-CK1.2-containing lysates to size-exclusion chromatography (SEC) and analysed
370 the distribution of the kinase across the elution profile. As shown in Figure 1B (blue circles),
371 L-CK1.2-V5 was recovered in fractions spanning from 8 mL to 20 mL. Apart from a strong enrichment
372 observed in fraction between 12 and 18 mL, the kinase was detectable evenly throughout most of the
373 fractions, indicating that the bulk of cellular L-CK1.2 is incorporated into large complexes rather than
374 existing as a free monomer. Indeed, the distribution of the total proteins is wider and detected up to
375 fraction 25 mL (Figure 1B, pink circles). Collectively, these data support the notion that *Leishmania*

376 CK1.2 predominantly participates in multi-protein complexes, underscoring the functional relevance of
377 protein-protein interactions for this kinase.

378 To identify the L-CK1.2 associated proteins (L-CKAP) influencing the regulation, functions or
379 subcellular localisation of this kinase, we used mock or CK1.2-V5-expressing *Ld*Bob cell line (18).
380 Three independent immuno-precipitations (IP) with logarithmic phase promastigotes (PRO) and axenic
381 amastigotes (axAMA Elution1, E1 & Elution 2, E2) cell lysates were performed using a mouse
382 monoclonal anti-V5 antibody. The eluted proteins were run on SDS-PAGE and analysed by quantitative
383 label-free mass spectrometry. We identified 1081 proteins in promastigote and 516 in amastigote, from
384 which respectively 645 (Figure 1Ca) and 341 (Figure 1Cb&c) were quantified (for the list of all
385 quantified proteins, see Table S1). In addition to L-CK1.2 itself, 84 proteins in PRO and 146 in axAMA
386 (Table S2) were selected as potential L-CKAPs, based on the following criteria: proteins identified with
387 2 or more distinct peptides, a fold change ratio CK1.2-V5/mock above 2 and a p-value below 0.05 in at
388 least two replicates (Figure 1Ca-c, red square and Table S2), as well as those uniquely identified in
389 CK1.2-V5 by at least 2 peptides or more in at least two replicates (Figure 1Ca-c, "only in CK1-V5" and
390 Table S2). Forty-two L-CKAPs were shared between both parasite stages (Table S2, green). Half of the
391 proteins identified in PRO and two third of those identified in AxAMA were stage-specific interactors
392 of L-CK1.2 in our conditions. The dissimilarity between the two developmental stages becomes even
393 more apparent when considering the enrichment of Gene Ontology (GO) terms associated with protein
394 class (see Figure S1B and Table S3, PANTHER: http://www.pantherdb.org/) or biological processes
395 (see Figure 1D, PANTHER: http://www.pantherdb.org/). In promastigotes, there is an over-
396 representation of terms like 'translational protein' (Figure S1B) and an exclusive representation of
397 'methylation' and 'ATP metabolic process' (Figure 1D). In axenic amastigotes, terms such as
398 'membrane traffic protein,' 'protein modifying enzyme,' and 'metabolite interconversion enzyme' exhibit
399 a higher representation (Figure S1B & Table S4) than in promastigotes, while terms such as 'vesicle-
400 mediated transport', 'exocytic process' and 'catabolic processes' (Figure 1D) are exclusively associated
401 with axenic amastigotes. These findings shed light on the potentially distinct functional characteristics
402 exhibited by L-CK1.2 in the two stages.

403

404 **L-CK1.2 localisation in *Leishmania* parasites is consistent with that of its interaction**
405 **partners.**

406 As the important cytoplasmic staining of L-CK1.2-V5 might mask other more specific localisations,
407 promastigotes were treated with 0,125% NP-40 to permeabilise membranes and facilitate the release of
408 the cytoplasmic pool of L-CK1.2, prior to PFA fixation and staining. The treatment conditions were
409 selected after optimisation steps performed to minimise the impact of the detergent on the nucleus and
410 kinetoplast morphology. We used organelle-specific markers for co-localisation with L-CK1.2 and also
411 to demonstrate the integrity of the organelle. We observed organelle-specific signals (i) adjacent to the
412 kinetoplast (Figure 2Aa, CK1.2-V5 & merge, white arrowhead), (ii) in the flagellar pocket region and
413 along the flagellum (Figure 2Aa, CK1.2-V5 & merge, yellow arrowhead and arrow, respectively), as
414 well as (iii) in the Hoechst-unstained region of the nucleus (Figure 2Aa, CK1.2-V5 & merge, white
415 arrow). Similar localisations were observed in axenic amastigotes (Figure 2Ab, CK1.2-V5 & merge).
416 These signals were reproducibly observed in all the samples that were analysed, including those fixed
417 with methanol (as an example: 3 min, Figure S2), suggesting that the observed localisation is not a
418 consequence of fixation processes. The organelle-specific localisation of L-CK1.2 might be due to
419 interactions with specific L-CKAPs. To determine the potential localisation of these interacting partners
420 in an exhaustive manner, we took advantage of the TrypTag (http://tryptag.org/ (40)), a community
421 database providing the localisation of most proteins encoded in the genome of *Trypanosoma brucei* and
422 we assumed that the L-CKAPs would have similar localisations than their syntenic *T. brucei* orthologs.
423 When possible, we confirmed the localisation with the LeishTag database
424 (https://www.leishtag.org/?pageType=landing). A total of 143 L-CKAPs were assigned subcellular
425 localisation using TrypTag (Table S2, column: *T. brucei* & localisation in *T. brucei* orthologs), and 20
426 using LeishTag (Table S2, column: localisation in *L. mexicana* paralog & *L. mexicana*). The remaining
427 24 proteins lacked localisation data in both databases, or had no ortholog in *T. brucei*. The Gene
428 Ontology enrichment for Cellular Component of the L-CKAPs was then established using the *T. brucei*
429 orthologs, which are better annotated and Revigo software (http://revigo.irb.hr/ (43)) of Tritrypdb. L-

430 CKAPs are localised in multiples organelles, including the cytosol, the nucleolus, the basal body, the
431 flagellum, the flagellar pocket, or the nuclear pore complex (Figure 2B & Table S5 (blue for PRO, red
432 for AxAMA and green for both)). Next, we performed co-localisation studies between L-CK1.2 and
433 marker proteins specific for these organelles to validate its pleiotropic localization.
434

435 **CK1.2 is localised in the granular zone of the nucleolus and redistributed to the mitotic**
436 **spindle during mitosis.**

437 Forty-eight L-CKAPs have a potential localisation to the nucleolus (Table S2 and S5). Most of L-CK1.2
438 interacting partners in the nucleolus are involved in translation, with a wide range of 40S and 60S
439 ribosomal proteins, as well as NOP56 (44). L-CK1.2 is also detected in the nucleolus as judged by
440 Figure 2Aa (CK1.2-V5, white arrow), where CK1.2-V5 is detected in a Hoechst-unstained, sub-nuclear
441 location. To confirm this result, the localisation of CK1.2-V5 in detergent-treated promastigotes was
442 compared to that of L1C6 antibody, which recognises an unknown nucleolar protein (45). As expected,
443 the L1C6-targeted antigen was detected in the centre of the nucleolus corresponding to the dense fibrillar
444 zone involved in rDNA transcription (Figure 3A, merged image, red staining) (46), confirming the
445 structural integrity of the nucleolus. In contrast, CK1.2-V5 was detected at the periphery of the
446 nucleolus, as dotted staining around L1C6 (Figure 3A, merged image, green staining). This region
447 corresponds to the granular component of the nucleolus, involved in the last steps of rRNA processing
448 and ribosome biogenesis. Our results indicate that CK1.2 might be involved in rRNA processing rather
449 than in rDNA transcription, which is consistent with its interaction with 40S and 60S ribosomal proteins,
450 as well as the NOP56, a nucleolar protein involved in ribosome biogenesis, which orchestrates the
451 correct assembly and the functioning of the box C/D small nucleolar ribonucleoproteins (snoRNPs) (44,
452 47-49). In addition to NOP56, L-CK1.2 interacts with members of NOP56 complex such as Fibrillarin
453 (box C/D snoRNPs), Hel67 (LSU assembly factors), 60S ribosomal L7 protein, GTP-binding nuclear
454 protein rtb2 and potentially the heat shock protein DNAJ (Figure 3B, (47)). Our interactome provides
455 additional evidence supporting the localization of L-CK1.2 to the nucleolus and suggests a role for L-
456 CK1.2 in ribosome processing.

457 The immunofluorescence experiment also unveils an additional function for nucleolar L-CK1.2. In
458 dividing cells, in contrast to the typical segregation pattern observed for nucleolar components
459 exemplified by L1C6 antigen (Figure 3C, red staining, panels a-f, and Figure S3A (50)), CK1.2 staining
460 elongates from a wheel-shaped to a bar-shaped configuration that spans the entire length of the nucleus,
461 following nucleolar elongation (Figure 3C, green staining, panels a-f, and Figure S3A). This localization
462 pattern bears a resemblance to that of the mitotic spindle, and we have evidence suggesting an interaction
463 between L-CK1.2 and α-tubulin, a component of the microtubules (Table S2). To determine whether L-
464 CK1.2 is localised to the spindle during chromosome segregation, we asked whether L-CK1.2 co-
465 localises with tubulin, a component of the spindle. As shown in Figure 3D (merged panels a-d) and
466 Figure S3B, CK1.2-V5 co-localises with tubulin and thus with the mitotic spindle in specific areas, an
467 observation supported by the mPc at or above 0.5 (Figure 3De, mitotic spindle).
468 During anaphase, CK1.2-V5 accumulates at each end of the elongated mitotic spindle (Figure 3Dc-
469 merge panel, white arrows; Figure S3Bd, white arrows), similarly to the twinfilin-like protein (51).
470 These findings suggest that *Leishmania* CK1.2 might play a role in regulating chromosome segregation
471 similarly to TbCK1.2 (51, 52). Consistent with this hypothesis, Nucleus and spindle associated protein
472 2 (LdNuSAP2), a highly divergent ortholog of Saccharomyces ASE1/HumanPRC1/ArabidopsisMAP65
473 protein family that mediates spindle elongation, was identified in L-CK1.2 interactome (53) alongside
474 eleven interacting partners of NuSAP2, suggesting that L-CK1.2 might be recruited to the spindle as
475 part of the NuSAP2 complex (Figure 3E, (53)). Further investigations will be required to determine the
476 mechanisms by which CK1.2 regulates mitosis.
477 A closer examination at potential complexes highlighted the specific association of CK1.2 with the
478 nuclear pore complex subunits in a life-stage specific manner (NPC, Figure 2B, grey square). While L-
479 CK1.2 interacts with only four NPC members in promastigotes (Figure S4C (blue squares) and Table
480 S5), it interacts with eighteen NPC subunits in axenic amastigotes (Figure S4C (blue and red squares)
481 and Table S5), including three hypothetical proteins. These proteins, LdBPK_091010.1,
482 LdBPK_100580.1, LdBPK_281740.1, might be novel components of the NPC, as judged by the
483 localization of their orthologs in *T. brucei* (40). These L-CKAPs cover most subcomplexes of the NPC
484 but are particularly enriched in the outer ring (Figure S4C), suggesting a tight, life-stage specific

485 interaction between L-CK1.2 and the nuclear pore in axenic amastigotes. Similarly to L-CK1.2, in
486 *Trypanosoma brucei*, CK1.2 interacts with TbNUP158, a member of the outer ring (54) and Hrr25, CK1
487 ortholog in *S. cerevisiae*, interacts with and phosphorylates NUP53(55).
488
489 **CK1.2 localises to the basal body and the flagellum.**
490 Based on GO enrichment analysis of cellular component (Figure 2B), 12 L-CKAPs (Table S5) are
491 predicted to locate to (i) the basal body that regulates flagellum duplication, (ii) the tripartite attachment
492 complex (TAC) that links the segregation of the kinetoplasts to that of the basal bodies, or (iii) the
493 transition fibers (TF), critical for flagellum assembly. Most of these interacting proteins were identified
494 either in axenic amastigotes or in both AxAMA and PRO, none were specific of PRO. Several of these
495 L-CKAPs are linked to the regulation of cell division and/or cytokinesis, such as *Leishmania* AKB1 or
496 KHAP2 (13, 56, 57), while other are members of the Tripartite Attachment Complex (TAC) such as
497 TAC60 (58). To determine whether L-CK1.2 localizes to these organelles, we selected two markers,
498 centrin-4 to investigate the potential localisation of CK1.2-V5 to the basal body (Figure 4A, CEN, white
499 arrow) and to the bilobe structure (Figure 4A, CEN, yellow arrow), and IFT172 to investigate the
500 potential localisation of CK1.2-V5 to the transition fibers (Figure 4A, IFT172) (59-61). As shown in
501 Figure 4A panel a, CK1.2-V5 does not co-localise neither with the kinetoplast DNA, as shown by the
502 mean Pearson correlation coefficient below 0.5 (mPc=0.27 ± 0.164, Figure 4B), nor with the bilobed
503 structure (Figure 4A panel a, yellow arrow and mPc of 0.47 ± 0.074, Figure 4B,). Instead, it co-localises
504 with centrin-4 to the basal bodies (Figure 4A panel a, white arrows and mPc of 0.741 ± 0.050, Figure
505 4B), and with IFT172 to the transition fibers, as judged by Figure 4A panel b, white arrow and confirmed
506 by an mPc of 0.805 ± 0.06 (Figure 4B), suggesting that L-CK1.2 might regulate flagellum duplication
507 as well as be loaded onto the flagellum. Consistent with this finding, we confirmed the localisation of
508 CK1.2-V5 to the axoneme (IFT172, Figure 4C, Merge and 3D-view), but not to the paraflagellar rod
509 (PFR2, Figure 4D, panel 3). Noticeably, the abundance of L-CK1.2 in the flagellum is lower than that
510 in the body of the parasite, which is consistent with the filtering existing at the entrance of the flagellum
511 (62). The flagellar localisation of L-CK1.2, which aligns with published proteomic data from *T. brucei*
512 and *Leishmania mexicana* flagellum (63, 64), as well as the identification of 19 flagellar L-CKAP (Table

513 S5, section flagellum, (64)) indicates a potential function for L-CK1.2 in the flagellum. Additionally,
514 L-CK1.2 phosphorylates HSP90 at Ser-289; blocking this modification, by introducing an S289A
515 mutation, produces mutant parasites whose flagella are shortened by roughly 50 % (20). This finding
516 suggests a regulatory role of L-CK1.2 in flagellar length.
517 Based on the literature and our findings, *Leishmania* promastigote, alongside *Chlamydomonas*
518 *reinhardtii* and *Trypanosoma brucei*, is one of the few eukaryotes exhibiting flagellar localization of
519 CK1 (65). In axenic amastigotes, however, CK1.2-V5 does not colocalise with IFT172, but instead
520 localises around the flagellum (Figure 4E, panel b and 3D view). These findings suggest that the role of
521 CK1.2 in the flagellum is more likely associated with motility or flagellum assembly than in sensing.
522

523 **_Leishmania_ CK1.2 interacts with host proteins.**

524 Several lines of evidence suggest that the L-CK1.2 is exported from the parasite in extracellular vesicles
525 (EVs) and can phosphorylate host substrates, thereby contributing to the parasite ability to subvert
526 macrophage biology (15, 19, 22). Because L-CK1.2 is expressed at low levels in both promastigotes
527 and axenic amastigotes(18), conventional immunoprecipitation (IP) of the kinase from infected
528 macrophages would not yield sufficient material for a comprehensive interactome analysis.
529 Furthermore, the amount of host-localised pool of L-CK1.2 that can be harvested from *Leishmania*-
530 infected BMDMs is well under the threshold needed for a robust IP-MS analysis. To circumvent these
531 limitations, we adopted an *in-vitro* pull-down strategy that has previously been validated for mapping
532 host–pathogen protein interactions in *Mycobacterium (66)*.

533 Recombinant L-CK1.2-V5, produced in *E. coli*, was incubated overnight with macrophage protein
534 lysates and immunoprecipitated using an anti-V5 antibody (18, 66) to identify the host L-CK1.2-
535 associated proteins (L-CKAP*host*) by mass spectrometry analysis. Two controls were added, an empty
536 vector, and a control-thioredoxin (an empty plasmid expressing thioredoxin-V5), as recombinant L-
537 CK1.2-V5 is fused to thioredoxin at the N-terminus to improve its solubility. Three independent
538 immuno-precipitations were performed using a mouse monoclonal anti-V5 antibody. The proteins were
539 run on SDS-PAGE (Figure 5Aa) and the binding partners revealed by quantitative label-free mass

540 spectrometry (Figure 5Aa, b &c). We identified 64 L-CKAP*host* in at least two replicates with at least
541 two distinct peptides detected (Table S6). L-CK1.2-V5 interacts with a wide range of host protein
542 classes, including chaperones and transporters, similar to the L-CKAPs identified in *Leishmania* (Figure
543 5B). This finding suggests that L-CK1.2 may perform similar functions in both the parasite and its host
544 cell. The GO analysis for Biological Process (Figure S5A) revealed a significant enrichment for the
545 terms 'purine biosynthetic process', 'glycolytic process' (ATP-dependent 6-phosphofructokinase, Pfkl
546 and Glyceraldehyde-3-phosphate dehydrogenase, Gapdh), 'mitochondrial electron transport'
547 (mitochondrial ATP synthase subunit, Atp5f1a, Atp5f1c and Atp5po, Cytochrome b-c1 complex subunit
548 8) and 'mitochondrial membrane respiratory chain' (Ndufa1, Ndufa10). These findings collectively
549 suggest a potential involvement of L-CK1.2 in reprogramming host cell energy metabolism, which
550 indeed undergoes a gradual shift from an M2-like respiratory metabolic state to an M1-like glycolytic
551 energy profile during *Leishmania* infection (67). We also identified an enrichment of GO terms
552 associated with infection, such as "immune response activation," "apoptotic cell death," and "response
553 to stress", suggesting a role for L-CK1.2 in subverting key host pathways that enable the parasite to
554 establish its niche and promote intracellular survival (Figure S5A, (68)).

555 Notably, many of the biological processes enriched in the interactome are also present in the L-CK1.2-
556 related host substratome we previously published (Figure S5B, Table S8 (19)). The most common
557 biological processes shared between the host interactome and the host substratome are related to post-
558 transcriptional regulation processes (Figure S5B, Table S8 (19)). Because of its potential dual role, L-
559 CK1.2 has the ability to function in both the parasite and the macrophage. To determine whether L-
560 CK1.2 targets the same pathways in both organisms, we analysed the intersection between biological
561 processes associated with L-CK1.2 in the parasite and the host cell by combining the L-CKAP*host* and
562 substratome datasets (this work and (19), Figure 5C, Table S7). Several biological processes were
563 conserved in both organisms, representing the core of L-CK1.2 functions: (i) biosynthetic metabolic
564 processes including RNA metabolic process and lipid biosynthetic process; (ii) translation; (iii) transport
565 including endocytosis, and trafficking; (iv) response to stimuli, regulation of cell communication and
566 signalling (Figure 5C). Another characteristic, conserved in both organisms, is protein folding, through
567 the interaction of L-CK1.2 with chaperone proteins (Figure 5B). We have shown that L-CK1.2 interacts

568 with *Leishmania* chaperone proteins, including HSP70s, HSP60, DNAJs, HSP110. Similarly in the
569 macrophage, L-CK1.2 interacts with DNAJs, Hspa5 (Hsp70) and Hsp90. Interestingly, while
570 *Leishmania* HSP90 is phosphorylated by L-CK1.2 (20), only host Hsp90 seems to interact with L-
571 CK1.2. Finally, to determine whether L-CK1.2 targets specific pathways in the parasite, we compared
572 the biological processes associated with L-CK1.2 in the parasite and the host cell by combining the L-
573 CKAP*host* and substratome datasets and retained those specific to the parasite (this work and (19),
574 Figure S5C, Table S9). The GO terms for several biological processes are specifically enriched in L-
575 CK1.2 parasite interactome, including 'precursor large subunit ribosomal RNA maturation', 'TOR
576 signalling' or 'cell cycle regulation' (Figure S5C, Table S9). Further investigations will be needed to
577 determine whether this specificity might arise from interactions with proteins absent in the host or from
578 differences in regulatory mechanisms.

579 Overall, although this experiment was conducted *in vitro* and may therefore capture interactions that do
580 not occur under physiological conditions, it generated a comprehensive catalogue of potential host
581 interacting partners of L-CK1.2. Notably, four proteins, Rcn2, Myo1f, Myo9b, and Hspa5, were
582 identified in both L-CK1.2 host interactome and substratome, making them particularly attractive targets
583 for further functional investigation (19).

584 **DISCUSSION**

585 Currently, little is known about *Leishmania* CK1.2, despite its crucial role in parasite survival and its
586 validation as a drug target (13, 18, 31), which might be linked to the challenges associated with studying
587 an essential signalling kinase. Our findings shed light on the versatile and essential nature of L-CK1.2,
588 demonstrated by its diverse subcellular localization and broad spectrum of interacting partners. We
589 showed that the known localisation of L-CK1.2 interacting partners is consistent with L-CK1.2
590 distribution, suggesting that these proteins may confer the necessary specificity for its functions. This
591 spatial coordination is particularly important given that L-CK1.2 is constitutively active (18). We
592 identified potential roles for L-CK1.2 in the parasite, including its involvement in translational
593 regulation, as evidenced by its interactions with numerous ribosomes and its involvement in molecular
594 transport across the nuclear envelope. Additionally, specifically in axenic amastigotes, L-CK1.2 might

595 play a role in vesicular trafficking, particularly endocytosis through its interaction with AP2 adaptor
596 protein complex. We are currently investigating this hypothesis.

597 We also identified host biological processes that may be regulated by L-CK1.2 through interactions with
598 host proteins, providing first insights into its potential role during infection. Many of the enriched host
599 processes in our dataset, including cell death, immune response, and transport, are known to be
600 modulated during *Leishmania* infection (69-72). The two main host processes targeted by L-CK1.2 seem
601 to be 'purine biosynthesis'', more specifically linked to 'glycolytic process', and mitochondrial electron
602 transport', indicating the potential involvement of L-CK1.2 in the regulation of the host respiratory
603 metabolism. This finding is consistent with recent data from Zhang *et al.* showing that macrophages
604 infected with *Leishmania amazonensis* shift towards aerobic glycolysis for ATP production (67).
605 Second, we identified many proteins linked to mitochondrial electron transport, particularly from the
606 complex I, such as Ndufa10, Ndufs1 and Ndufs3, subunits of the mitochondrial membrane respiratory
607 chain NADH dehydrogenase, important to maintain the mitochondrial membrane potential. *Leishmania*
608 is known to target host mitochondria to modulate survival and also to control mitochondrial
609 bioenergetics (73). Consistent with a role for L-CK1.2 in this process during *Leishmania* infection,
610 human CK1δ/CK1ε have been involved in the regulation of complexes I and IV of the electron transport
611 chain (74). The release of L-CK1.2 in the host cell via extracellular vesicles, as well as its ability to
612 interact with and phosphorylate host proteins, suggest a dual role for L-CK1.2, in both the parasite and
613 the host cell to regulate intracellular parasite survival (this work, (15, 19, 22)). Unlike viruses or bacteria
614 that hijack host CK1 to manipulate cellular functions, *Leishmania* secretes its own CK1, suggesting that
615 L-CK1.2 can functionally replace its mammalian counterparts. Supporting this hypothesis, our previous
616 work demonstrated that the first 325 of the 353 amino acids, encompassing the catalytic domain and
617 part of the C-terminus, are fully conserved among human-infecting *Leishmania* species, establishing L-
618 CK1.2 as the most conserved kinase across these parasites (18). This conservation, unaffected by
619 geographical diversity or differences in insect vectors, is likely driven by strong selective pressure from
620 mammalian host cells on the L-CK1.2 protein sequence, explaining its high similarity to human
621 orthologs (12, 18). However, this similarity does not extend to the C-terminus, suggesting that this

622 domain might not be important for L-CK1.2 host functions. This hypothesis is not supported by the high
623 conservation of L-CK1.2 C-terminal domain in most *Leishmania* species infecting humans (12, 18).
624 One possible explanation lies in the presence of Low Complexity Regions (LCRs) within this domain.
625 LCRs have been shown to be more abundant in highly connected proteins, such as signaling kinases,
626 and contribute to protein interactions (75). Notably, LCRs are also found in the C-terminal domains of
627 human CK1α, CK1δ, CK1ε, CK1γ1, CK1γ2, and CK1γ3 (Figure S6, http://smart.embl-
628 heidelberg.de/smart/set_mode.cgi?NORMAL=1, (76)). This conservation is striking, given the
629 divergence of the L-CK1.2 C-terminus from its mammalian counterparts, suggesting that LCRs may be
630 the key elements enabling L-CK1.2 to recognize proteins in the parasite and in the host. These protein-
631 protein interactions are crucial, as L-CK1.2 is devoid of signal peptide or any similar domains (12, 18),
632 and thus likely relies on host interacting partners to reach the subcellular localisation to exert its
633 functions, like its mammalian orthologs(17). Conceivably, blocking these interactions might prevent L-
634 CK1.2 functions in the host cell likely reducing parasite survival, a possibility we are currently
635 investigating.

636 Another puzzling question is why *Leishmania* parasites would release an ortholog of kinases already
637 present in the host cell, rather than subvert host CK1 like viruses or bacteria (77, 78)? Is L-CK1.2 in
638 competition with the host CK1s? We hypothesize that during *Leishmania* infection, the functions
639 targeted by L-CK1.2 might be attenuated by the inhibition or the reduced abundance of the host CK1s.
640 One publication supports this hypothesis: Isnard *et al.* showed that CK1α, presents in the nucleus of host
641 macrophage, decreases in abundance during *L. major* or *L. mexicana* infection (79). Interestingly,
642 human CK1α phosphorylates IFNAR1/2 leading to its degradation (19, 22) and the removal of the
643 interferon α and β receptor from the plasma membrane. This example shows that during infection while
644 the macrophage would need to decrease CK1α to maintain those receptors at the cell surface and
645 perceive the extracellular environment, the parasite would rather remove them by secreting its own CK1
646 to ensure that the macrophage is unaware of its environment, thus creating a safe niche for the parasite.
647 Moreover, whereas the mammalian Ck1α, Ck1δ, and Ck1ε are autoinhibited and need the interactions

648 with other proteins, such as Ddx3, for its activation, L-CK1.2 does not require interacting partners for
649 its activity (18, 80).

650 One conserved feature of L-CK1.2 between the parasite and the host is its interaction with heat shock
651 proteins, suggesting that L-CK1.2 might particularly contribute to the response to environmental cues.
652 We, as well as other previously published studies, clearly show a strong link between L-CK1.2 and heat
653 shock proteins of the parasite. L-CK1.2 is in complex with the *Leishmania* HSP70s and phosphorylates
654 HSP23, P23 and HSP90, (this study, (20, 21)). The regulation of HSP23 and p23 is linked to temperature
655 tolerance, while the phosphorylation of Hsp90 on Ser289 is important for parasite growth, flagella length
656 and morphology (20, 21). Unexpectedly, we did not identify HSP90 among the L-CKAPs despite its
657 abundance or any proteins involved in the foldosome, such as STI1 (81). This finding contrasts with
658 human CK1s, which phosphorylate Hsp70 and Hsp90 to regulate the balance between protein folding
659 and degradation (82), or whose abundance is regulated by Hsp90 (83). Noticeably, while *Leishmania*
660 HSP90 was not identified among the L-CKAPs, host Hsp90ab1 was identified among the L-CKAP*host*
661 (this work and (19)), suggesting that its HSP90-related functions may differ between the parasite and
662 the macrophage, potentially resembling those of mammalian CK1s more closely. The importance of L-
663 CK1.2 interaction with *Leishmania* HSP70 is unclear. HSP70 is part of a super family with several
664 paralogs displaying different localisations such as the cytoplasm (HSPA1A), the lumen of the
665 endoplasmic reticulum (HSPA5) or the mitochondrion (HSPA9A) (84). According to our data, L-CK1.2
666 interacts with several *Leishmania* HSP70 paralogs, although assigning a paralog was impossible due to
667 the high percentage of identity between the different members. L-CK1.2 might also interact with host
668 Hspa5, an endoplasmic reticulum chaperone involved in protein folding and quality control.

669 Our study provides extensive amount of data but has certain limitations, particularly regarding the host
670 dataset, which was derived from macrophage lysates and does not account for localization constraints.
671 Despite this limitation, protein class ontology analysis shows that our host dataset aligns well with the
672 parasite dataset, which was obtained by tagging L-CK1.2 within the parasite. Future research will focus
673 on validating these interactions in more physiological contexts, such as a cellular model or infected
674 macrophages. Tracking the localization of L-CK1.2 in macrophages would be highly informative,

675 though challenging due to its high similarity to host CK1s. We already know that the mouse anti-CK1
676 antibody cross-reacts with L-CK1.2, and our attempts to use a custom-made L-CK1.2 antibody for
677 immunofluorescence have been unsuccessful. Additionally, tagging CK1.2 in the parasite with GFP or
678 similarly sized fluorophores has proven ineffective, as it disrupts kinase function, limiting our options.

679

680 **CONCLUSION**

681 Studying signalling kinases is inherently challenging, as their impairment affects multiple pathways,
682 making it difficult to dissect precise regulatory mechanisms. Our study addresses this challenge by
683 identifying specific interacting partners of L-CK1.2, which will be instrumental in elucidating its diverse
684 functions in the parasite. Our findings highlight CK1.2 as a pivotal enzyme required not only for the
685 survival of *Leishmania* but also for its successful adaptation to the host cell environment. We propose
686 that this parasite-encoded serine/threonine kinase exerts dual functionality, acting in cis within the
687 parasite itself while simultaneously operating in trans within the macrophage. In doing so, CK1.2 might
688 establish itself as a bidirectional signalling hub that coordinates communication between pathogen and
689 host. These findings position CK1.2 as a critical molecular effector that drives macrophage subversion
690 and ultimately facilitates the establishment and persistence of infection ((15), this work). Furthermore,
691 given the close relationship between *Leishmania* CK1.2 and its orthologs in *Trypanosoma brucei*
692 (TbCK1.2), *Trypanosoma cruzi* (TcCK1.2), *Toxoplasma gondii* (TgCK1α), and *Plasmodium falciparum*
693 (PfCK1)(18), our findings are likely to have broader implications for other parasitic infections.

694

695

696 **Funding**

697 This work was supported by the ANR-13-ISV3-0009 (to N.R.), by "Région Ile-de-France" and
698 Fondation pour la Recherche Médicale grants (to D.L.). Daniel Martel was supported by the French
699 Government's Investissements d'Avenir program Laboratoire d'Excellence Integrative Biology of
700 Emerging Infectious Diseases (to N.R., grant no. ANR-10-LABX-62-IBEID studentship).

Acknowledgments

The authors would like to thanks Hira L Nakhasi, U.S. FDA, for the anti-*Ld*centrin antibody; Philippe Bastin, Institut Pasteur, for the anti-*Tb*IFT172 and anti-*Tb*PFR2 (L8C4) antibodies; Keith Gull, University of Oxford for the L1C6 antibody; the Unit of Technology and Service - Photonic BioImaging (UTechS PBI) from the Institut Pasteur and the Image Analysis Hub of the Institut Pasteur for the help with confocal microscopy and analyses of co-localisations, in particular Audrey Salles, Julien Fernandes, Anne Danckaert and Jean-Yves Tinevez. Finally, we would like to thank Brice Rotureau, Thierry Blisnick and Philippe Bastin for fruitful discussions and advice.

Author contribution

Conceptualization: NR; Investigation: DM, OL and NR; Formal analysis: DM, OL, FD, VL, DL and NR; Writing - original draft: DM and NR; Writing - review & Editing: DM, OL, FD, VL, DL, GFS and NR; Funding acquisition: GFS and NR; Supervision NR.

714 # Figure legends

715 **FIGURE 1: *Leishmania* CK1.2 displays a pleiotropic localisation and interacts with numerous**
716 **proteins in promastigotes and in axenic amastigotes**

717 **(A)** IFA of *Ld*Bob pLEXSY-CK1.2-V5 (a) and *Ld*Bob pLEXSY (mock, b) promastigotes, fixed with
718 PFA. The confocal images show the anti-V5 staining (CK1.2-V5 or V5, green), Hoechst 33342 staining
719 (H, blue), a merge and the transmission image (Trans). Scale bar, 2 µm. The pictures are maximum
720 intensity projection of the confocal stacks containing the parasites. (c) IFA of *Ld*Bob pLEXSY-CK1.2-
721 V5 axenic amastigotes, fixed with PFA. The single channel images show CK1.2-V5 (green) and Hoechst
722 33342 (H, blue) signals, the merge and the transmission image (Trans). Scale bar, 2 µm. The pictures
723 are maximum intensity projection of the confocal stacks containing the parasites. Confocal stacks were
724 deconvolved and corrected for chromatic aberration. The images presented in Figure 1A are
725 representatives of at least 3 replicates. **(B)** Size-exclusion chromatography (SEC) of L-CK1.2-V5-
726 containing complexes. 3.5 mg of protein, extracted in native conditions from *Ld*Bob pLEXSY-CK1.2-
727 V5 (blue line) were separated by SEC on a superose 6 increase 10/300 GL columns. Fractions of 200 µl
728 were collected and 15 µl of each fraction was separated by SDS-PAGE in denaturing conditions and
729 analysed by Western blotting using an anti-V5 antibody (bottom panel). A blot for each strain,
730 representative of the three replicates, is presented in the bottom panel. The quantification of the three
731 replicates (dotted, dashed and plain lines) using the chemidoc imaging system (Biorad) is presented in
732 the top panel. Each vertical line represents a fraction (from A1 to H12). MW= Molecular Weight. **(C)**
733 Volcano plots representing the changes in protein abundance of LCKAPs in PRO (a), AxAMA elution
734 E1 (b) and E2 (c). Proteins were selected if identified with at least 2 peptides in at least 2 replicates
735 either only in the L-CK1.2-V5 conditions, or with a fold change above 2 and a p-value ≤ 0.05 compared
736 to the mock conditions. Proteins highlighted in red are those with at least 2 distinct peptides in at least
737 2 replicates. **(D)** GO term enrichment for the 'biological process' in promastigotes and axenic
738 amastigotes performed using PANTHER.db (http://www.pantherdb.org/, see also Table S4).

739 **FIGURE 2: L-CK1.2 localisation in *Leishmania* parasites is consistent with that of its interaction**
740 **partners.**
741 **(A)** IFA of *Ld*Bob pLEXSY-CK1.2-V5 promastigotes (a) and axenic amastigotes (b) obtained after
742 detergent treatment followed by PFA fixation. Similar to **(Figure 1A)**, except that the images are sum
743 intensity projection of the confocal stacks containing the parasites. The images presented in Figure 2A
744 are representatives of at least 3 replicates. **(B)** Graphical representation of the GO term enrichment for
745 cellular component from the *Trypanosoma brucei* orthologs of both PRO and AxAMA interacting
746 proteins using cytoscape app, Revigo (43) and tritrypdb GO enrichment (https://tritrypdb.org). The
747 dataset of *Trypanosoma brucei* TREU927 has been used. The color of the node represents the (Log10(p-
748 value), between value from - 25.55 to - 1.3). The size of the nodes represents the log size, which is the
749 Log10(Number of annotations for GO Term ID in selected species in the EBI GOA database). Three
750 percent of the strongest GO term pairwise similarities are designated as edges (grey) in the graph (43).
751 The grey square highlights the nuclear pore complex.
752
753 **FIGURE 3: CK1.2 localises in the nucleolus and to the mitotic spindle.**
754 **(A)** IFA pictures of *Ld*Bob pLEXSY-CK1.2-V5 promastigotes obtained after detergent treatment
755 followed by PFA fixation. The images show the single channel images of the transmission image
756 (Trans), CK1.2-V5, Hoechst 33342 (H, blue) and L1C6 signals (red) and merged image. The right panel
757 show a magnification of the nucleus region. Scale bar, 2 µm. These pictures are single stacks extracted
758 from deconvolved confocal stacks corrected for chromatic aberration. **(B)** Subunits of NOP56 complex
759 implicated in ribosomal subunits biogenesis found in our dataset. Fill colors: Green, detected in
760 promastigotes; Yellow, detected in axenic amastigotes; and Green/Yellow, present in both life stage.
761 Border colors: Red, corresponds to box C/D snoRNPs; Purple, corresponds to LSU assembly factors;
762 Blue, putative ribosome assembly factors; and Black, potential interaction found in this study. **(C)** IFA
763 pictures of *Ld*Bob pLEXSY-CK1.2-V5 promastigotes obtained after detergent treatment followed by
764 PFA fixation and stained with anti-V5 (CK1.2-V5) and anti-L1C6 (nucleolus, L1C6) antibodies.
765 Confocal images representing sequential events of mitosis revealed different localisation patterns of
766 L1C6 nucleolar marker and CK1.2-V5. (a – f) The images show the merged image containing CK1.2-

767 V5 (green), Hoechst 33342 (H) (blue) and L1C6 (red) signals and a magnification of the nuclear region.
768 N=nucleus, K=kinetoplast. Scale bar, 2 µm or 1 µm for magnified images. These pictures are single
769 stacks extracted from deconvolved confocal stacks corrected for chromatic aberration. See also Figure
770 S3A. **(D)** IFA pictures of *Ld*Bob pLEXSY-CK1.2-V5 promastigotes obtained after detergent treatment
771 followed by PFA fixation and stained with anti-V5 and anti-α-tubulin antibodies. Sequential images of
772 various stages of cell division (a – d) showing the single channel images for α-tubulin signals and the
773 merged images showing CK1.2-V5 (green), H (blue) and α-tubulin (red) signals. Scale bar, 2 µm. These
774 pictures are single stacks extracted from deconvolved confocal stacks corrected for chromatic
775 aberration. See also Figure S3B. (e) Dot plots showing Pearson's covariation coefficients for different
776 combination of signals in the entire mitotic spindle region and in a reduced mitotic spindle region
777 containing also CK1.2-V5 signal. Regions of the spindle containing both CK1.2-V5 and tubulin were
778 selected to evaluate whether L-CK1.2 localises to the spindle using Pearson's covariation coefficients.
779 For both regions, CK1.2-V5 signal was compared with α-tubulin (TUB) or Hoechst 33342 (H). The
780 signal of TUB was also compared with H. Pearson's covariation coefficients were measured from n=7
781 different confocal stacks which were deconvolved and corrected for chromatic aberration with Huygens
782 Professional software. The plot was generated with GraphPad Prism software and the mean values are
783 represented with red bold segments. **(E)** Subunits of NuSAP2 complex, found in our dataset, implicated
784 in chromosome segregation. Fill colors: Green, detected in promastigotes; Yellow, detected in axenic
785 amastigotes; and Green/Yellow, present in both life stage. Border colors: Black, potential interaction
786 found in this study. The images presented in Figure 3 are representatives of at least 3 replicates.
787

788 **FIGURE 4: CK1.2 is localised to the basal bodies and the flagellum.**
789 **(A)** IFA of *Ld*Bob pLEXSY-CK1.2-V5 promastigotes obtained after detergent treatment followed by
790 PFA fixation. Single channel images of the CK1.2-V5, Hoechst 33342 (H), centrin 4 (CEN) or IFT172
791 signals and the transmission image (Trans). The white arrow highlights the basal bodies and the yellow
792 arrow the bilobe region. The merge panel shows CK1.2-V5 signal (green) merged with H (Hoechst
793 33342, blue), CEN (centrin 4, red) and IFT172 (cyan). The two right panels show a magnification of

794 region 1 with H signal (blue) merged with (a) CK1.2-V5 (green) and CEN (red) and (b) IFT172 (red)
795 and CK1.2-V5 (green) signals. Scale bar, 2 µm or 1 µm for magnified images. These pictures are single
796 stacks extracted from deconvolved confocal stacks corrected for chromatic aberration. The white arrows
797 highlight the basal bodies and the yellow arrow the bilobe region. **(B)** Dot plots showing Pearson's
798 covariation coefficients in the basal body (BB) or the flagellar pocket (FP) regions for different
799 combination of signals. Pearson's covariation coefficients were measured from n=14 different confocal
800 stacks which were deconvolved and corrected for chromatic aberration with Huygens Professional
801 software. The plot was generated with GraphPad Prism software and the mean values are represented
802 with red bold segments. **(C)** IFA of *Ld*Bob pLEXSY-CK1.2-V5 promastigotes fixed by PFA and stained
803 with the anti-V5 and anti-IFT172 antibodies. The left panels display the single channel images of the
804 CK1.2-V5, IFT172, Hoechst 33342 (H) signals, the transmission image (Trans), and a merge of CK1.2-
805 V5 (green), IFT172 (red) and H (blue) signals. The right panel shows a 3D-reconstruction (3D view) of
806 the flagellum (image 2), with CK1.2-V5 signal (green) merged with IFT172 (red). **(D)** IFA of *Ld*Bob
807 pLEXSY-CK1.2-V5 promastigotes obtained after detergent treatment followed by PFA fixation and
808 staining with the anti-V5 and anti-PFR2 antibodies. The following images show CK1.2-V5, PFR2,
809 Hoechst 33342 (H) signals, the transmission image (Trans), and finally the merge of CK1.2-V5 (green),
810 PFR2 (red) and H (blue) signals. (image 3) 3D-reconstruction (3D view) of the flagellum (white square
811 in (merge)), showing CK1.2-V5 signal (green) merged with PFR2 (red). Scale bars, 2 µm or 1 µm for
812 2D images. Pictures in (E) and (D, left panels) are single stacks extracted from deconvolved confocal
813 stacks corrected for chromatic aberration. All confocal stacks containing the parasite were used for
814 pictures (D, image 2 and E image 3). **(E)** IFA of *Ld*Bob pLEXSY-CK1.2-V5 axenic amastigotes
815 obtained after detergent treatment followed by PFA fixation. The single channel and the merge images
816 show CK1.2-V5, Hoechst 33342 (H, blue), centrin 4 (CEN, red) or IFT172 (cyan) signals and the
817 transmission image (Trans). Scale bar, 2 µm. These pictures are single stacks extracted from
818 deconvolved confocal stacks corrected for chromatic aberration. Panel a shows a merged of CK1.2-V5,
819 Hoechst 33342 (H, blue) and centrin 4 (CEN, red); Panel b shows CK1.2-V5, Hoechst 33342 (H, blue),
820 and IFT172 (cyan) signals; 3D-reconstruction of the flagellar pocket region and its neck from image

821 (Figure 5Fa and b), which has been rotated. All confocal z-stacks containing the parasite were used for
822 the 3D view. The images presented in Figure 4 are representatives of at least 3 replicates.
823
824 **FIGURE 5: L-CK1.2 interacts with macrophage proteins.**
825 **(A)** The recombinant L-CK1.2-V5, the control-thioredoxin and the control were incubated overnight
826 with BMDM protein lysates and immunoprecipitated using an anti-V5 antibody. The proteins were
827 eluted by two successive elutions with glycine elution buffer (elution 1 and 2) followed by one elution
828 with NuPAGE loading buffer (elution 3). Proteins from elutions 1 and 3 were used for MS analysis
829 (Figure 5A a, b and c). Volcano plots representing the changes in protein abundance of L-CK1.2 vs
830 control (a), of L-CK1.2 vs control thioredoxin (b) and of control thioredoxin vs control (c), including
831 all the proteins identified with 1 peptide in at least 1 replicate. Proteins highlighted in red are those with
832 at least 2 distinct peptides in at least 2 replicates. **(B)** Graphical representation of the affinity purification
833 merged with the string app to visualise protein-protein interactions for host proteins using the cytoscape
834 app. The classification in different categories is based on GO terms enrichment. The colour of the nodes
835 represents the Fold change (see the legend on the figure). **(C)** GO term enrichment for the 'biological
836 process' common between the host cell and *Leishmania donovani* performed using the cytoscape app
837 (see also Table S7).
838
839

840 # References

841 1. Knippschild U, Kruger M, Richter J, Xu P, Garcia-Reyes B, Peifer C, et al. The CK1
842 Family: Contribution to Cellular Stress Response and Its Role in Carcinogenesis. Front Oncol.
843 2014;4:96.
844 2. Greer YE, Westlake CJ, Gao B, Bharti K, Shiba Y, Xavier CP, et al. Casein kinase
845 1delta functions at the centrosome and Golgi to promote ciliogenesis. Molecular biology of the
846 cell. 2014;25(10):1629-40.
847 3. Greer YE, Rubin JS. Casein kinase 1 delta functions at the centrosome to mediate Wnt-
848 3a-dependent neurite outgrowth. J Cell Biol. 2011;192(6):993-1004.
849 4. Peng Y, Moritz M, Han X, Giddings TH, Lyon A, Kollman J, et al. Interaction of
850 CK1delta with gammaTuSC ensures proper microtubule assembly and spindle positioning.
851 Molecular biology of the cell. 2015b;26(13):2505-18.
852 5. Bozatzi P, Sapkota GP. The FAM83 family of proteins: from pseudo-PLDs to anchors
853 for CK1 isoforms. Biochemical Society transactions. 2018;46(3):761-71.

854 6. Hu Y, Liu X, Lu Q, Yang Y, He Q, Liu Y, et al. FRQ-CK1 Interaction Underlies
855 Temperature Compensation of the Neurospora Circadian Clock. mBio. 2021;12(3):e0142521.
856 7. Wolff S, Xiao Z, Wittau M, Sussner N, Stoter M, Knippschild U. Interaction of casein
857 kinase 1 delta (CK1 delta) with the light chain LC2 of microtubule associated protein 1A
858 (MAP1A). Biochimica et biophysica acta. 2005;1745(2):196-206.
859 8. Knippschild U, Gocht A, Wolff S, Huber N, Lohler J, Stoter M. The casein kinase 1
860 family: participation in multiple cellular processes in eukaryotes. Cell Signal. 2005;17(6):675-
861 89.
862 9. Schittek B, Sinnberg T. Biological functions of casein kinase 1 isoforms and putative
863 roles in tumorigenesis. Mol Cancer. 2014;13:231.
864 10. Jiang S, Zhang M, Sun J, Yang X. Casein kinase 1alpha: biological mechanisms and
865 theranostic potential. Cell Commun Signal. 2018;16(1):23.
866 11. Bhattacharya D, Ansari IH, Striker R. The flaviviral methyltransferase is a substrate of
867 Casein Kinase 1. Virus Res. 2009;141(1):101-4.
868 12. Rachidi N, Knippschild U, Späth GF. Dangerous Duplicity: The Dual Functions of
869 Casein Kinase 1in Parasite Biology and Host Subversion. Frontiers in Cellular and Infection
870 Microbiology. 2021;11(230).
871 13. Baker N, Catta-Preta CMC, Neish R, Sadlova J, Powell B, Alves-Ferreira EVC, et al.
872 Systematic functional analysis of Leishmania protein kinases identifies regulators of
873 differentiation or survival. Nat Commun. 2021;12(1):1244.
874 14. Dan-Goor M, Nasereddin A, Jaber H, Jaffe CL. Identification of a secreted casein kinase
875 1 in Leishmania donovani: effect of protein over expression on parasite growth and virulence.
876 PloS one. 2013;8(11):e79287.
877 15. Silverman JM, Clos J, de'Oliveira CC, Shirvani O, Fang Y, Wang C, et al. An exosome-
878 based secretion pathway is responsible for protein export from Leishmania and communication
879 with macrophages. J Cell Sci. 2010;123(Pt 6):842-52.
880 16. Atayde VD, Suau HA, Townsend S, Hassani K, Kamhawi S, Olivier M. Exosome
881 secretion by the parasitic protozoan Leishmania within the sand fly midgut. Cell reports.
882 2015;13(5):957-67.
883 17. Xu P, Ianes C, Gartner F, Liu C, Burster T, Bakulev V, et al. Structure, regulation, and
884 (patho-)physiological functions of the stress-induced protein kinase CK1 delta (CSNK1D).
885 Gene. 2019;715:144005.
886 18. Rachidi N, Taly JF, Durieu E, Leclercq O, Aulner N, Prina E, et al. Pharmacological
887 assessment defines the Leishmania donovani casein kinase 1 as a drug target and reveals
888 important functions in parasite viability and intracellular infection. Antimicrob Agents
889 Chemother. 2014;58(3).
890 19. Smirlis D, Dingli F, Sabatet V, Roth A, Knippschild U, Loew D, et al. Identification of
891 the Host Substratome of Leishmania-Secreted Casein Kinase 1 Using a SILAC-Based
892 Quantitative Mass Spectrometry Assay. Frontiers in cell and developmental biology.
893 2021;9:800098.
894 20. Hombach-Barrigah A, Bartsch K, Smirlis D, Rosenqvist H, MacDonald A, Dingli F, et
895 al. Leishmania donovani 90 kD Heat Shock Protein - Impact of Phosphosites on Parasite
896 Fitness, Infectivity and Casein Kinase Affinity. Scientific reports. 2019;9(1):5074.
897 21. Kröber-Boncardo C, Lorenzen S, Brinker C, Clos J. Casein kinase 1.2 over expression
898 restores stress resistance to Leishmania donovani HSP23 null mutants. Scientific reports.
899 2020;10(1):15969.
900 22. Liu J, Carvalho LP, Bhattachariya S, Carbone CJ, Kumar KG, Leu NA, et al.
901 Mammalian casein kinase 1alpha and its leishmanial ortholog regulate stability of IFNAR1 and
902 Type I interferon signaling. Mol Cell Biol. 2009;29(24):6401-12.

23. Martel D, Beneke T, Gluenz E, Spath GF, Rachidi N. Characterisation of Casein Kinase 1.1 in Leishmania donovani Using the CRISPR Cas9 Toolkit. BioMed research international. 2017;2017:4635605.
24. Florimond C, Sahin A, Vidilaseris K, Dong G, Landrein N, Dacheux D, et al. BILBO1 Is a Scaffold Protein of the Flagellar Pocket Collar in the Pathogen Trypanosoma brucei. PLoS pathogens. 2015;11(3):e1004654.
25. Selvapandiyan A, Duncan R, Debrabant A, Bertholet S, Sreenivas G, Negi NS, et al. Expression of a mutant form of Leishmania donovani centrin reduces the growth of the parasite. J Biol Chem. 2001;276(46):43253-61.
26. Absalon S, Blisnick T, Kohl L, Toutirais G, Dore G, Julkowska D, et al. Intraflagellar transport and functional analysis of genes required for flagellum formation in trypanosomes. Mol Biol Cell. 2008;19(3):929-44.
27. Kohl L, Sherwin T, Gull K. Assembly of the Paraflagellar Rod and the Flagellum Attachment Zone Complex During the Trypanosoma brucei Cell Cycle. Journal of Eukaryotic Microbiology. 1999;46(2):105-9.
28. Devaux S, Kelly S, Lecordier L, Wickstead B, Perez-Morga D, Pays E, et al. Diversification of function by different isoforms of conventionally shared RNA polymerase subunits. Mol Biol Cell. 2007;18(4):1293-301.
29. Hombach A, Ommen G, Chrobak M, Clos J. The Hsp90–Sti1 interaction is critical for Leishmania donovani proliferation in both life cycle stages. Cellular Microbiology. 2013;15(4):585-600.
30. Schindelin J, Arganda-Carreras I, Frise E, Kaynig V, Longair M, Pietzsch T, et al. Fiji: an open-source platform for biological-image analysis. Nature methods. 2012;9(7):676-82.
31. Durieu E, Prina E, Leclercq O, Oumata N, Gaboriaud-Kolar N, Vougogiannopoulou K, et al. From Drug Screening to Target Deconvolution: a Target-Based Drug Discovery Pipeline Using Leishmania Casein Kinase 1 Isoform 2 To Identify Compounds with Antileishmanial Activity. Antimicrobial Agents and Chemotherapy. 2016;60(5):2822-33.
32. Aulner N, Danckaert A, Rouault-Hardoin E, Desrivot J, Helynck O, Commere PH, et al. High content analysis of primary macrophages hosting proliferating Leishmania amastigotes: application to anti-leishmanial drug discovery. PLoS Negl Trop Dis. 2013;7(4):e2154.
33. Poullet P, Carpentier S, Barillot E. myProMS, a web server for management and validation of mass spectrometry-based proteomic data. PROTEOMICS. 2007;7(15):2553-6.
34. The M, MacCoss MJ, Noble WS, Kall L. Fast and Accurate Protein False Discovery Rates on Large-Scale Proteomics Data Sets with Percolator 3.0. J Am Soc Mass Spectrom. 2016;27(11):1719-27.
35. Valot B, Langella O, Nano E, Zivy M. MassChroQ: a versatile tool for mass spectrometry quantification. Proteomics. 2011;11(17):3572-7.
36. Perez-Riverol Y, Bandla C, Kundu DJ, Kamatchinathan S, Bai J, Hewapathirana S, et al. The PRIDE database at 20 years: 2025 update. Nucleic acids research. 2025;53(D1):D543-D53.
37. Mi H, Ebert D, Muruganujan A, Mills C, Albou LP, Mushayamaha T, et al. PANTHER version 16: a revised family classification, tree-based classification tool, enhancer regions and extensive API. Nucleic acids research. 2021;49(D1):D394-D403.
38. Aslett M, Aurrecoechea C, Berriman M, Brestelli J, Brunk BP, Carrington M, et al. TriTrypDB: a functional genomic resource for the Trypanosomatidae. Nucleic acids research. 2010;38(Database issue):D457-62.
39. Szklarczyk D, Kirsch R, Koutrouli M, Nastou K, Mehryary F, Hachilif R, et al. The STRING database in 2023: protein-protein association networks and functional enrichment

952 analyses for any sequenced genome of interest. Nucleic acids research. 2023;51(D1):D638-
953 D46.
954 40. Dean S, Sunter JD, Wheeler RJ. TrypTag.org: A Trypanosome Genome-wide Protein
955 Localisation Resource. Trends in Parasitology. 2017;33(2):80-2.
956 41. Szklarczyk D, Gable AL, Lyon D, Junge A, Wyder S, Huerta-Cepas J, et al. STRING
957 v11: protein-protein association networks with increased coverage, supporting functional
958 discovery in genome-wide experimental datasets. Nucleic acids research. 2019;47(D1):D607-
959 D13.
960 42. Shannon P, Markiel A, Ozier O, Baliga NS, Wang JT, Ramage D, et al. Cytoscape: a
961 software environment for integrated models of biomolecular interaction networks. Genome
962 Res. 2003;13(11):2498-504.
963 43. Supek F, Bosnjak M, Skunca N, Smuc T. REVIGO summarizes and visualizes long lists
964 of gene ontology terms. PloS one. 2011;6(7):e21800.
965 44. Nepomuceno-Mejia T, Florencio-Martinez LE, Martinez-Calvillo S. Nucleolar Division
966 in the Promastigote Stage of Leishmania major Parasite: A Nop56 Point of View. BioMed
967 research international. 2018;2018:1641839.
968 45. Názer E, Sánchez DO. Nucleolar Accumulation of RNA Binding Proteins Induced by
969 ActinomycinD Is Functional in Trypanosoma cruzi and Leishmania mexicana but Not in T.
970 brucei. PloS one. 2011;6(8):e24184.
971 46. Motta MCM, Souza Wd, Thiry M. Immunocytochemical detection of DNA and RNA
972 in endosymbiont-bearing trypanosomatids. FEMS Microbiology Letters. 2003;221(1):17-23.
973 47. Nepomuceno-Mejia T, Florencio-Martinez LE, Pineda-Garcia I, Martinez-Calvillo S.
974 Identification of factors involved in ribosome assembly in the protozoan parasite Leishmania
975 major. Acta Trop. 2022;228:106315.
976 48. Kiss-Laszlo Z, Henry Y, Bachellerie JP, Caizergues-Ferrer M, Kiss T. Site-specific
977 ribose methylation of preribosomal RNA: a novel function for small nucleolar RNAs. Cell.
978 1996;85(7):1077-88.
979 49. Galardi S, Fatica A, Bachi A, Scaloni A, Presutti C, Bozzoni I. Purified box C/D
980 snoRNPs are able to reproduce site-specific 2'-O-methylation of target RNA in vitro. Mol Cell
981 Biol. 2002;22(19):6663-8.
982 50. Ogbadoyi E, Ersfeld K, Robinson D, Sherwin T, Gull K. Architecture of the
983 Trypanosoma brucei nucleus during interphase and mitosis. Chromosoma. 2000;108(8):501-
984 13.
985 51. Kumar G, Kajuluri LP, Gupta CM, Sahasrabuddhe AA. A twinfilin-like protein
986 coordinates karyokinesis by influencing mitotic spindle elongation and DNA replication in
987 Leishmania. Mol Microbiol. 2016;100(1):173-87.
988 52. Urbaniak MD. Casein kinase 1 isoform 2 is essential for bloodstream form
989 Trypanosoma brucei. Molecular and Biochemical Parasitology. 2009;166(2):183-5.
990 53. Zhou Q, Lee KJ, Kurasawa Y, Hu H, An T, Li Z. Faithful chromosome segregation in
991 Trypanosoma brucei requires a cohort of divergent spindle-associated proteins with distinct
992 functions. Nucleic acids research. 2018;46(16):8216-31.
993 54. Moreira C, Kelemen CD, Obado SO, Zahedifard F, Zhang N, Holetz FB, et al. Impact
994 of inherent biases built into proteomic techniques: Proximity labeling and affinity capture
995 compared. J Biol Chem. 2023;299(1):102726.
996 55. Lusk CP, Waller DD, Makhnevych T, Dienemann A, Whiteway M, Thomas DY, et al.
997 Nup53p is a target of two mitotic kinases, Cdk1p and Hrr25p. Traffic. 2007;8(6):647-60.
998 56. Inoue M, Okamoto K, Uemura H, Yasuda K, Motohara Y, Morita K, et al. Identification
999 and characterization of a cell division-regulating kinase AKB1 (associated kinase of
1000 Trypanosoma brucei 14-3-3) through proteomics study of the Tb14-3-3 binding proteins.
1001 Journal of biochemistry. 2015;158(1):49-60.

1002 57. Kelly FD, Tran KD, Hatfield J, Schmidt K, Sanchez MA, Landfear SM. A cytoskeletal
1003 protein complex is essential for division of intracellular amastigotes of Leishmania mexicana.
1004 J Biol Chem. 2020;295(37):13106-22.
1005 58. Kaser S, Willemin M, Schnarwiler F, Schimanski B, Poveda-Huertes D, Oeljeklaus S,
1006 et al. Biogenesis of the mitochondrial DNA inheritance machinery in the mitochondrial outer
1007 membrane of Trypanosoma brucei. PLoS pathogens. 2017;13(12):e1006808.
1008 59. Vaughan S, Gull K. Basal body structure and cell cycle-dependent biogenesis in
1009 Trypanosoma brucei. Cilia. 2015;5:5.
1010 60. Selvapandiyan A, Kumar P, Morris JC, Salisbury JL, Wang CC, Nakhasi HL, et al.
1011 Centrin1 Is Required for Organelle Segregation and Cytokinesis in Trypanosoma brucei.
1012 Molecular Biology of the Cell. 2007;18(9):3290-301.
1013 61. Shi J, Franklin JB, Yelinek JT, Ebersberger I, Warren G, He CY. Centrin4 coordinates
1014 cell and nuclear division in T. brucei. Journal of cell science. 2008;121(Pt 18):3062-70.
1015 62. Bertiaux E, Bastin P. Dealing with several flagella in the same cell. Cell Microbiol.
1016 2020;22(3):e13162.
1017 63. Subota I, Julkowska D, Vincensini L, Reeg N, Buisson J, Blisnick T, et al. Proteomic
1018 analysis of intact flagella of procyclic Trypanosoma brucei cells identifies novel flagellar
1019 proteins with unique sub-localization and dynamics. Molecular & cellular proteomics : MCP.
1020 2014;13(7):1769-86.
1021 64. Beneke T, Demay F, Hookway E, Ashman N, Jeffery H, Smith J, et al. Genetic
1022 dissection of a Leishmania flagellar proteome demonstrates requirement for
1023 directional motility in sand fly infections. bioRxiv. 2018:476994.
1024 65. Boesger J, Wagner V, Weisheit W, Mittag M. Application of phosphoproteomics to find
1025 targets of casein kinase 1 in the flagellum of chlamydomonas. International journal of plant
1026 genomics. 2012;2012:581460.
1027 66. Bach H, Papavinasasundaram KG, Wong D, Hmama Z, Av-Gay Y. Mycobacterium
1028 tuberculosis virulence is mediated by PtpA dephosphorylation of human vacuolar protein
1029 sorting 33B. Cell Host Microbe. 2008;3(5):316-22.
1030 67. Zhang S. LL, Varet H., Legendre R., Mahtal N., Proux C., Aulner N., Shorte S.,
1031 Granjean C., Bousso P., Prina E., Späth G.F. The m6A reader IGF2BP2 directs immune-
1032 metabolic reprogramming in Leishmania amazonensis-infected macrophages. bioRxiv June
1033 2024.
1034 68. Smirlis D, Dingli F, Pescher P, Prina E, Loew D, Rachidi N, et al. SILAC-based
1035 quantitative proteomics reveals pleiotropic, phenotypic modulation in primary murine
1036 macrophages infected with the protozoan pathogen Leishmania donovani. Journal of
1037 proteomics. 2020;213:103617.
1038 69. Gupta P, Srivastav S, Saha S, Das PK, Ukil A. Leishmania donovani inhibits
1039 macrophage apoptosis and pro-inflammatory response through AKT-mediated regulation of
1040 beta-catenin and FOXO-1. Cell Death Differ. 2016;23(11):1815-26.
1041 70. Solano-Galvez SG, Alvarez-Hernandez DA, Gutierrez-Kobeh L, Vazquez-Lopez R.
1042 Leishmania: manipulation of signaling pathways to inhibit host cell apoptosis. Ther Adv Infect
1043 Dis. 2021;8:20499361211014977.
1044 71. Rossi M, Fasel N. How to master the host immune system? Leishmania parasites have
1045 the solutions! Int Immunol. 2018;30(3):103-11.
1046 72. Singh AK, Pandey RK, Siqueira-Neto JL, Kwon YJ, Freitas-Junior LH, Shaha C, et al.
1047 Proteomic-based approach to gain insight into reprogramming of THP-1 cells exposed to
1048 Leishmania donovani over an early temporal window. Infect Immun. 2015;83(5):1853-68.
1049 73. Moreira D, Rodrigues V, Abengozar M, Rivas L, Rial E, Laforge M, et al. Leishmania
1050 infantum modulates host macrophage mitochondrial metabolism by hijacking the SIRT1-
1051 AMPK axis. PLoS pathogens. 2015;11(3):e1004684.

1052 74. Burger KL, Fernandez MR, Meads MB, Sudalagunta P, Oliveira PS, Renatino
1053 Canevarolo R, et al. CK1delta and CK1epsilon Signaling Sustains Mitochondrial Metabolism
1054 and Cell Survival in Multiple Myeloma. Cancer Res. 2023;83(23):3901-19.
1055 75. Coletta A, Pinney JW, Solis DY, Marsh J, Pettifer SR, Attwood TK. Low-complexity
1056 regions within protein sequences have position-dependent roles. BMC systems biology.
1057 2010;4:43.
1058 76. Schultz J, Milpetz F, Bork P, Ponting CP. SMART, a simple modular architecture
1059 research tool: identification of signaling domains. Proceedings of the National Academy of
1060 Sciences of the United States of America. 1998;95(11):5857-64.
1061 77. Xia C, Wolf JJ, Vijayan M, Studstill CJ, Ma W, Hahm B. Casein Kinase 1alpha
1062 Mediates the Degradation of Receptors for Type I and Type II Interferons Caused by
1063 Hemagglutinin of Influenza A Virus. J Virol. 2018;92(7).
1064 78. Jayaswal S, Kamal MA, Dua R, Gupta S, Majumdar T, Das G, et al. Identification of
1065 Host-Dependent Survival Factors for Intracellular Mycobacterium tuberculosis through an
1066 siRNA Screen. PLoS pathogens. 2010;6(4):e1000839.
1067 79. Isnard A, Christian JG, Kodiha M, Stochaj U, McMaster WR, Olivier M. Impact of
1068 Leishmania infection on host macrophage nuclear physiology and nucleopore complex
1069 integrity. PLoS pathogens. 2015;11(3):e1004776.
1070 80. Dolde C, Bischof J, Gruter S, Montada A, Halekotte J, Peifer C, et al. A CK1 FRET
1071 biosensor reveals that DDX3X is an essential activator of CK1epsilon. J Cell Sci. 2018;131(1).
1072 81. Morales MA, Watanabe R, Dacher M, Chafey P, Osorio y Fortea J, Scott DA, et al.
1073 Phosphoproteome dynamics reveal heat-shock protein complexes specific to the Leishmania
1074 donovani infectious stage. Proceedings of the National Academy of Sciences of the United
1075 States of America. 2010;107(18):8381-6.
1076 82. Muller P, Ruckova E, Halada P, Coates PJ, Hrstka R, Lane DP, et al. C-terminal
1077 phosphorylation of Hsp70 and Hsp90 regulates alternate binding to co-chaperones CHIP and
1078 HOP to determine cellular protein folding/degradation balances. Oncogene. 2012.
1079 83. Sharma K, Vabulas RM, Macek B, Pinkert S, Cox J, Mann M, et al. Quantitative
1080 proteomics reveals that Hsp90 inhibition preferentially targets kinases and the DNA damage
1081 response. Molecular & cellular proteomics : MCP. 2012;11(3):M111 014654.
1082 84. Drini S, Criscuolo A, Lechat P, Imamura H, Skalicky T, Rachidi N, et al. Species- and
1083 Strain-Specific Adaptation of the HSP70 Super Family in Pathogenic Trypanosomatids.
1084 Genome Biol Evol. 2016;8(6):1980-95.

1085

Figure 1

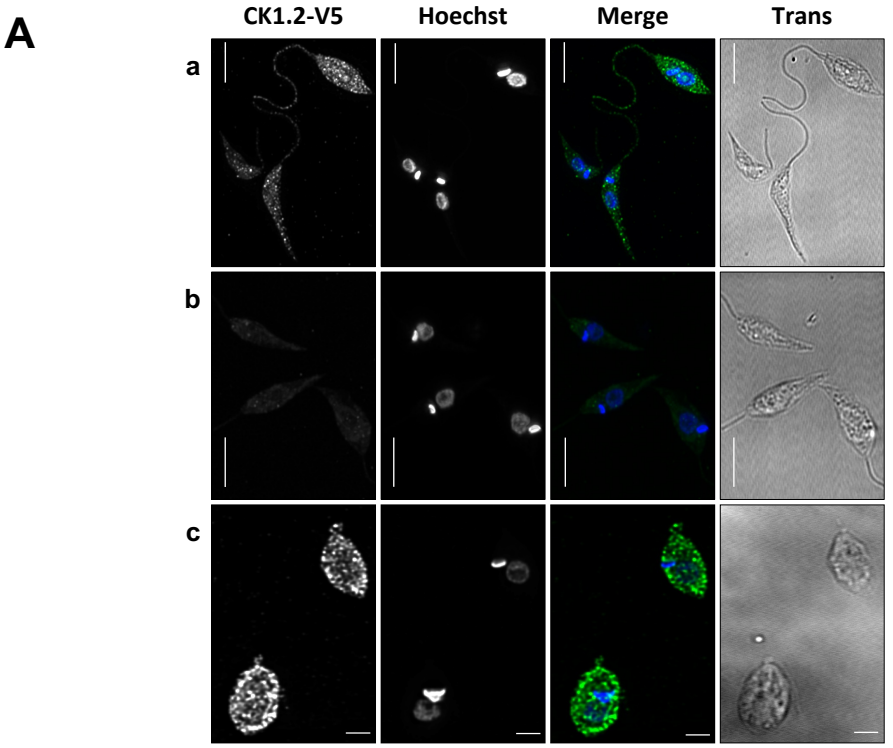
A
CK1.2-V5
Hoechst
Merge
Trans
a
b
c

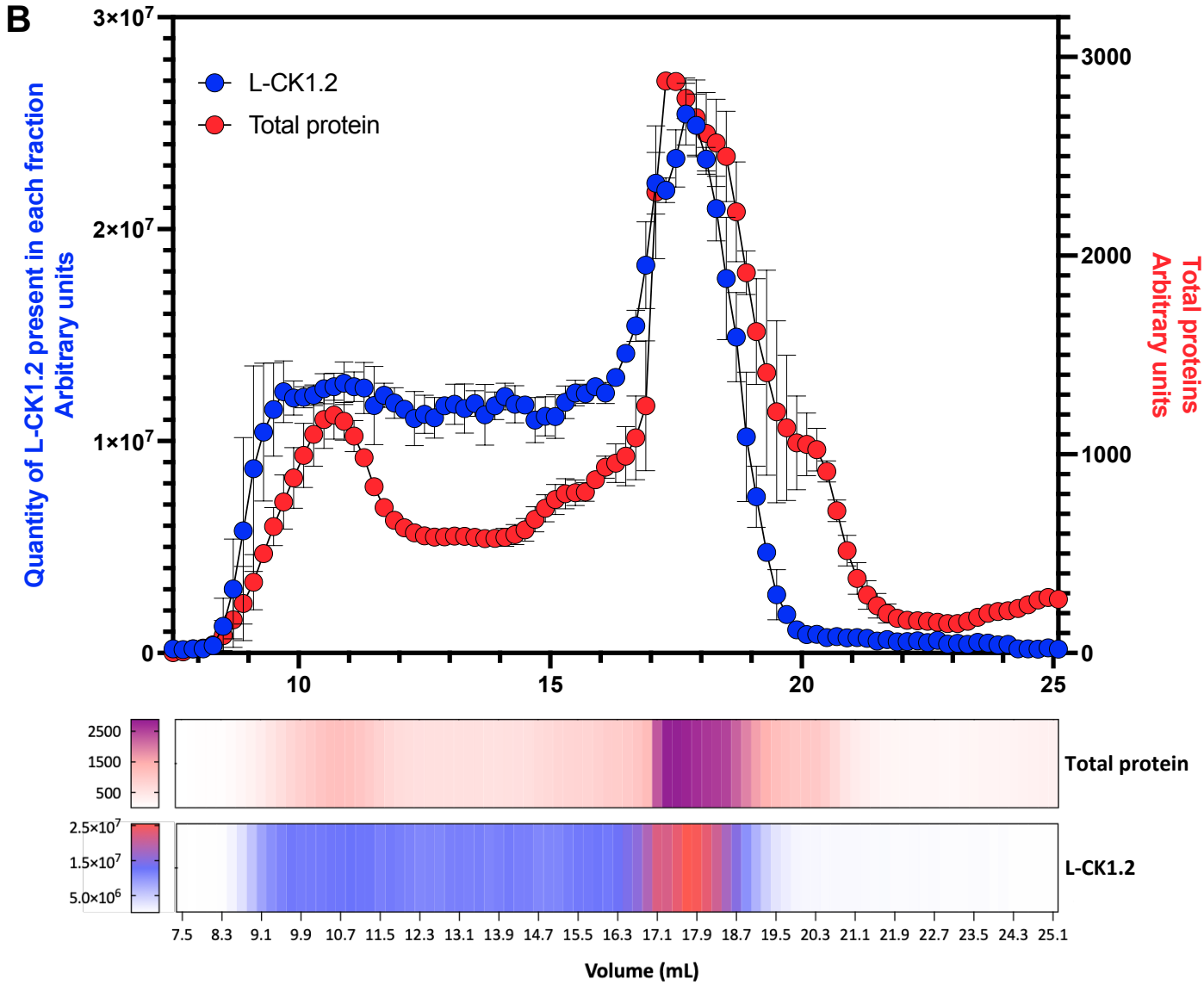
B
L-CK1.2
Total protein
Quantity of L-CK1.2 present in each fraction
Arbitrary units
Total proteins
Arbitrary units
3×10^7
2×10^7
1×10^7
0
3000
2000
1000
0
10
15
20
25
2500
1500
500
Total protein
2.5×10^7
1.5×10^7
5.0×10^6
L-CK1.2
7.5 8.3 9.1 9.9 10.7 11.5 12.3 13.1 13.9 14.7 15.5 16.3 17.1 17.9 18.7 19.5 20.3 21.1 21.9 22.7 23.5 24.3 25.1
Volume (mL)

Figure 1

C

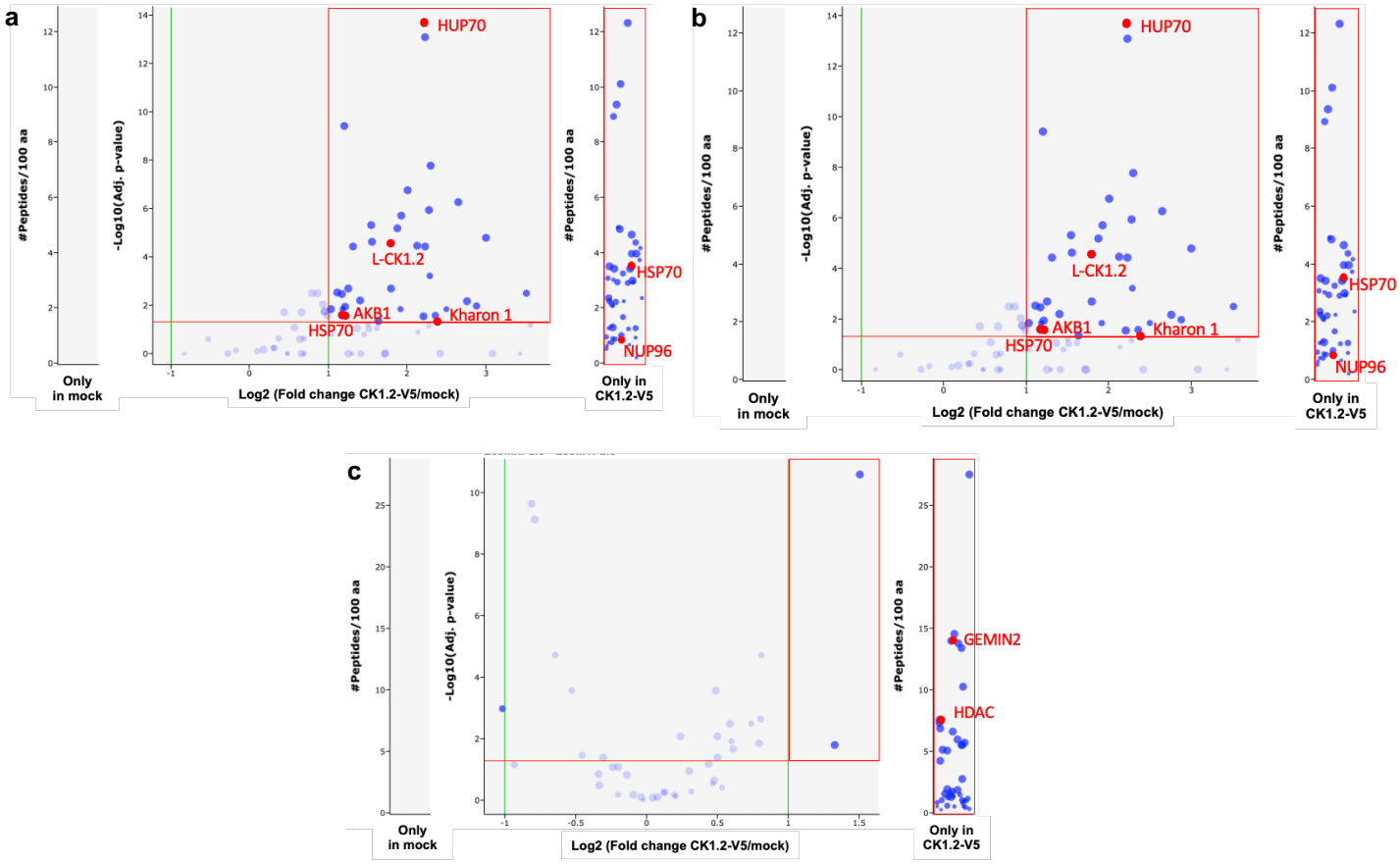
a
b
c
#Peptides/100 aa
-Log10(Adj. p-value)
Log2 (Fold change CK1.2-V5/mock)
Only in mock
Only in CK1.2-V5
HUP70
L-CK1.2
AKB1
Kharon 1
HSP70
NUP96
GEMIN2
HDAC

D

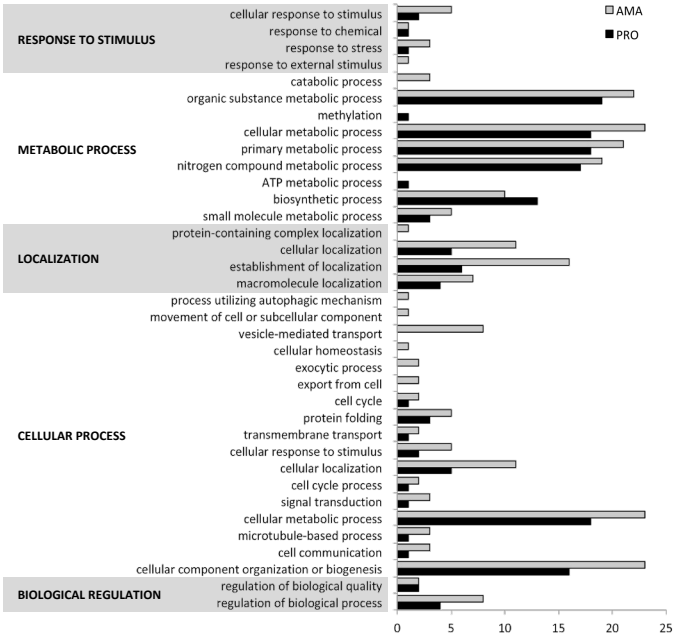
AMA
PRO
RESPONSE TO STIMULUS
cellular response to stimulus
response to chemical
response to stress
response to external stimulus
METABOLIC PROCESS
catabolic process
organic substance metabolic process
methylation
cellular metabolic process
primary metabolic process
nitrogen compound metabolic process
ATP metabolic process
biosynthetic process
small molecule metabolic process
LOCALIZATION
protein-containing complex localization
cellular localization
establishment of localization
macromolecule localization
CELLULAR PROCESS
process utilizing autophagic mechanism
movement of cell or subcellular component
vesicle-mediated transport
cellular homeostasis
exocytic process
export from cell
cell cycle
protein folding
transmembrane transport
cellular response to stimulus
cellular localization
cell cycle process
signal transduction
cellular metabolic process
microtubule-based process
cell communication
cellular component organization or biogenesis
BIOLOGICAL REGULATION
regulation of biological quality
regulation of biological process
0
5
10
15
20
25

Figure 2

A

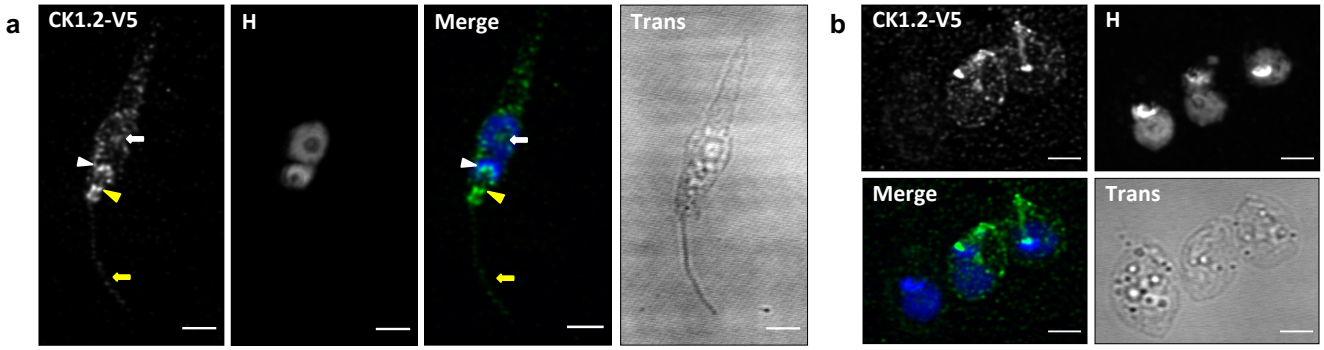
a
CK1.2-V5
H
Merge
Trans
b
CK1.2-V5
H
Merge
Trans

B

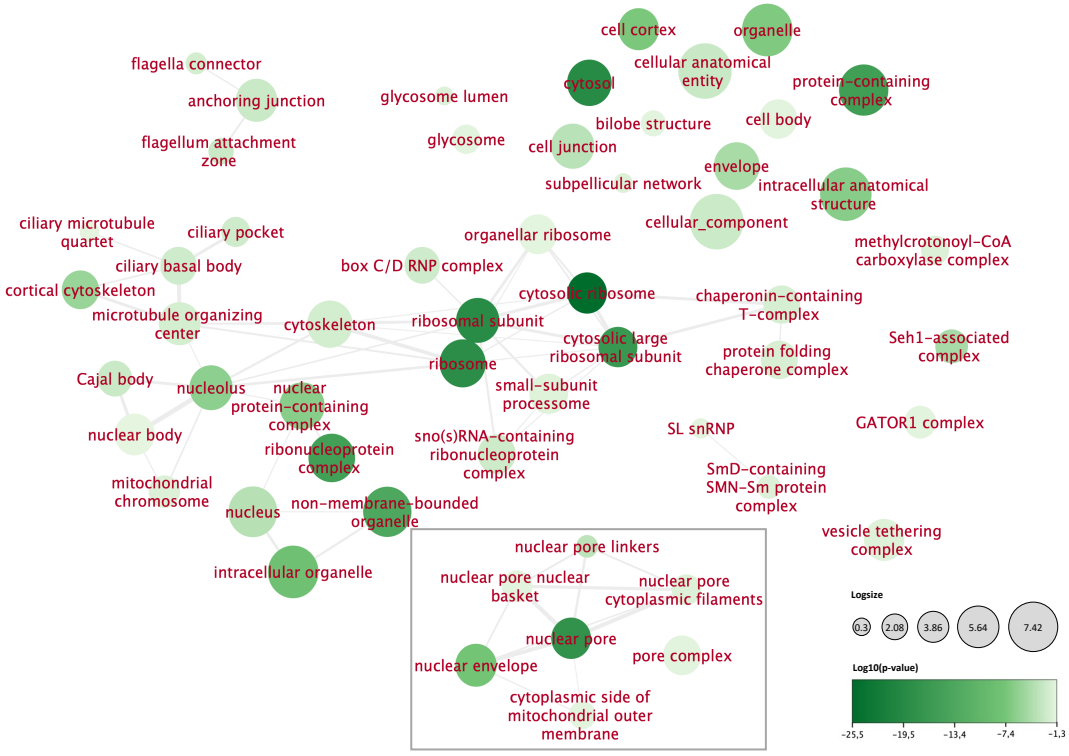
cell cortex
organelle
flagella connector
cellular anatomical entity
cytosol
protein-containing complex
anchoring junction
glycosome lumen
bilobe structure
cell body
flagellum attachment zone
glycosome
cell junction
envelope
subpellicular network
intracellular anatomical structure
ciliary microtubule quartet
ciliary pocket
organellar ribosome
cellular_component
methylcrotonoyl-CoA carboxylase complex
ciliary basal body
box C/D RNP complex
cortical cytoskeleton
cytosolic ribosome
chaperonin-containing T-complex
microtubule organizing center
cytoskeleton
ribosomal subunit
cytosolic large ribosomal subunit
protein folding chaperone complex
Seh1-associated complex
ribosome
Cajal body
nucleolus
nuclear protein-containing complex
small-subunit processome
nuclear body
ribonucleoprotein complex
sno(s)RNA-containing ribonucleoprotein complex
SL snRNP
GATOR1 complex
mitochondrial chromosome
nucleus
non-membrane-bounded organelle
SmD-containing SMN-Sm protein complex
vesicle tethering complex
intracellular organelle
nuclear pore linkers
nuclear pore nuclear basket
nuclear pore cytoplasmic filaments
nuclear pore
nuclear envelope
pore complex
cytoplasmic side of mitochondrial outer membrane
Logsize
0.3
2.08
3.86
5.64
7.42
Log10(p-value)
-25,5
-19,5
-13,4
-7,4
-1,3

Figure 3

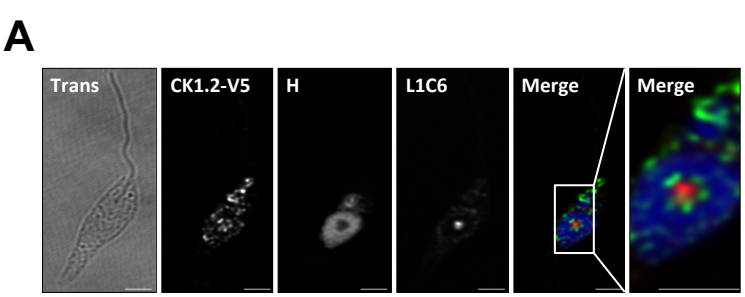
A
Trans
CK1.2-V5
H
L1C6
Merge
Merge

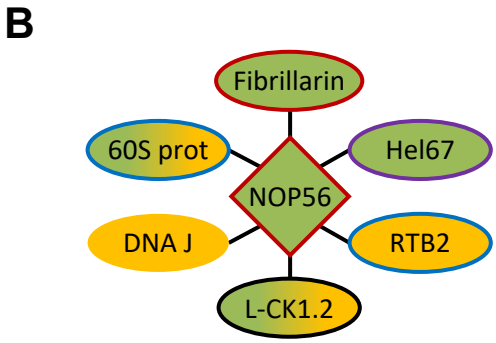
B
Fibrillarin
60S prot
Hel67
NOP56
DNA J
RTB2
L-CK1.2

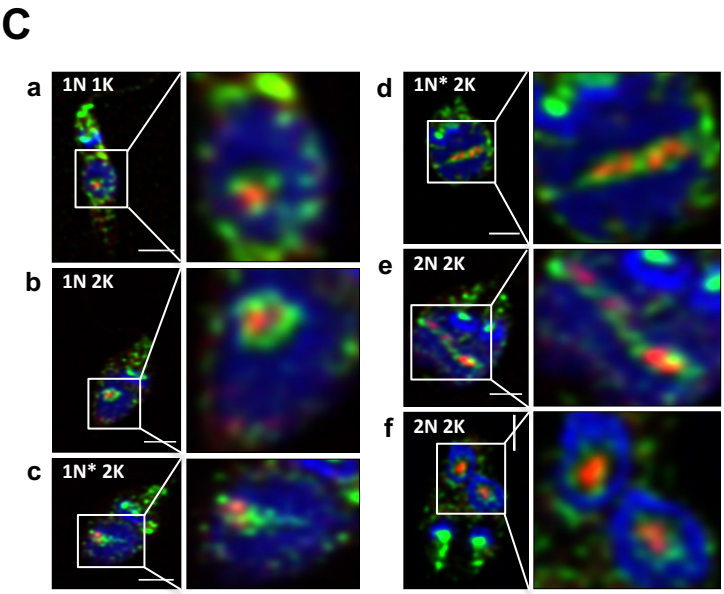
C
a
1N 1K
b
1N 2K
c
1N* 2K
d
1N* 2K
e
2N 2K
f
2N 2K

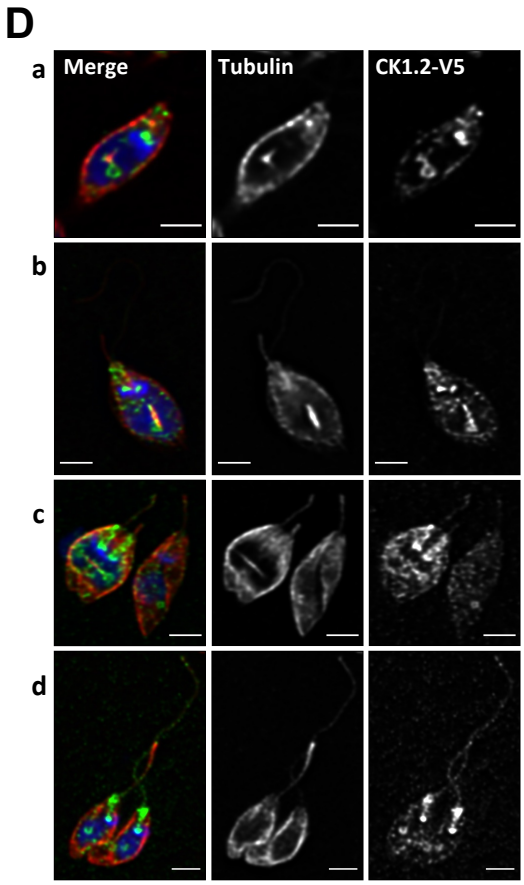
D
a
Merge
Tubulin
CK1.2-V5
b
c
d

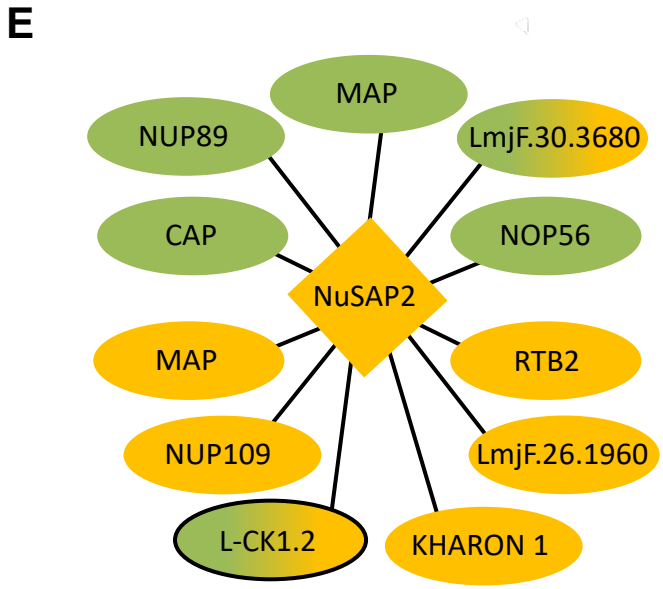
E
MAP
NUP89
LmjF.30.3680
CAP
NOP56
NuSAP2
MAP
RTB2
NUP109
LmjF.26.1960
L-CK1.2
KHARON 1

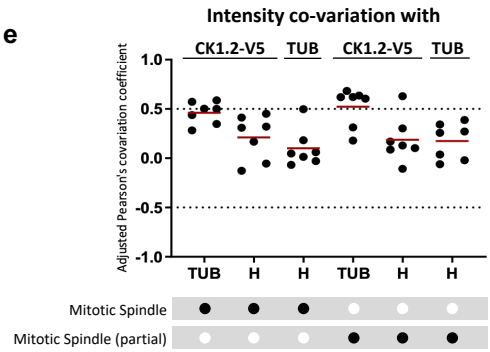
e
Intensity co-variation with
CK1.2-V5
TUB
CK1.2-V5
TUB
Adjusted Pearson's covariation coefficient
1.0
0.5
0.0
-0.5
-1.0
TUB
H
H
TUB
H
H
Mitotic Spindle
Mitotic Spindle (partial)

Figure 4

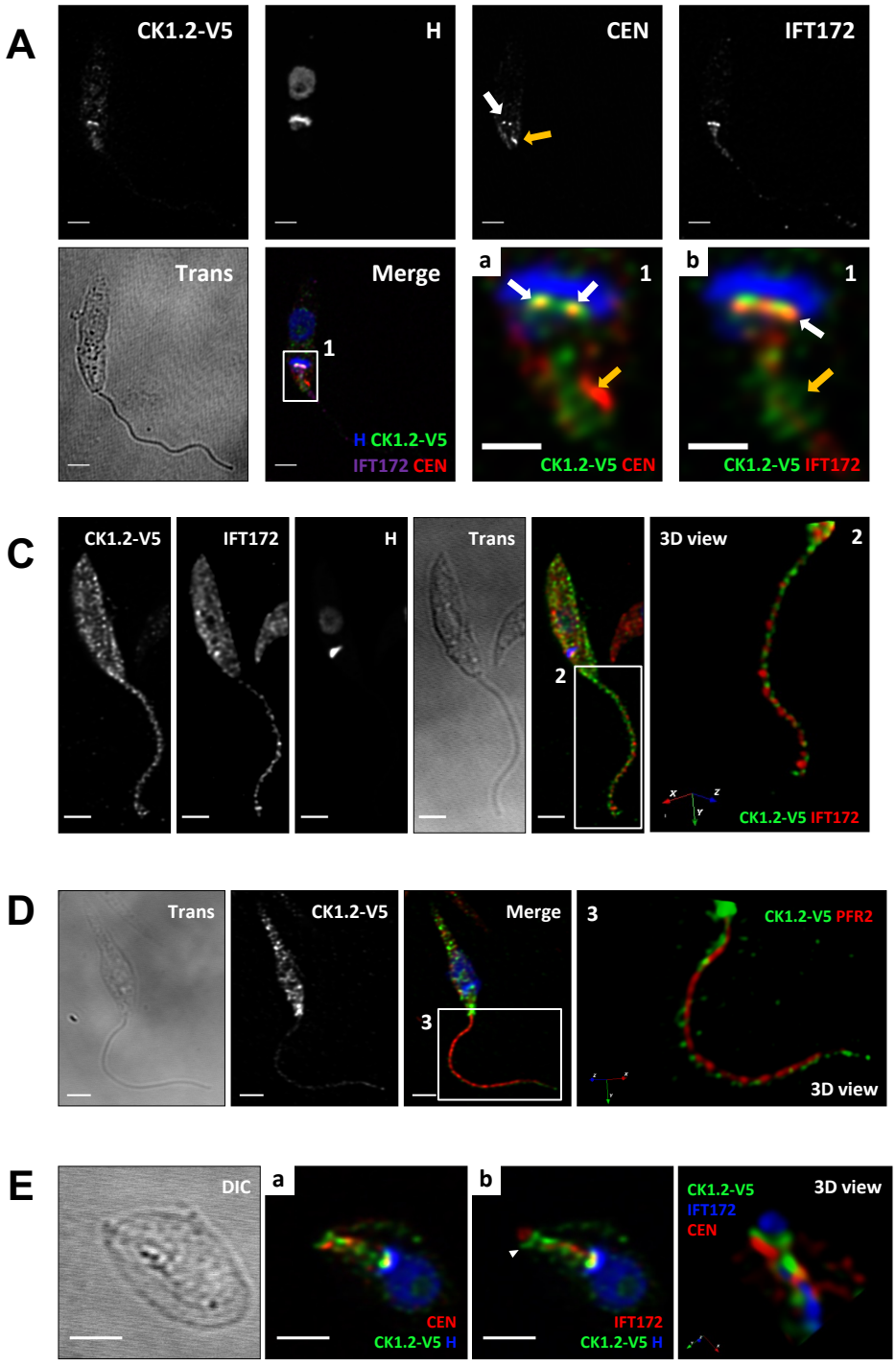
A
CK1.2-V5
H
CEN
IFT172
Trans
Merge
1
H CK1.2-V5
IFT172 CEN
a
1
CK1.2-V5 CEN
b
1
CK1.2-V5 IFT172
C
CK1.2-V5
IFT172
H
Trans
2
3D view
2
CK1.2-V5 IFT172
D
Trans
CK1.2-V5
Merge
3
3
CK1.2-V5 PFR2
3D view
E
DIC
a
CEN
CK1.2-V5 H
b
IFT172
CK1.2-V5 H
CK1.2-V5
IFT172
CEN
3D view

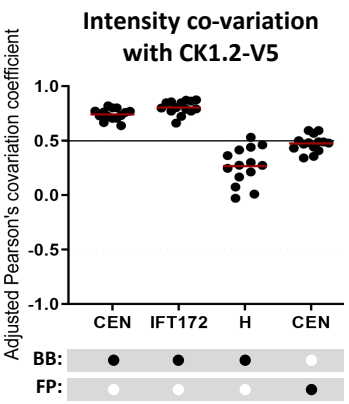
B
Intensity co-variation with CK1.2-V5
Adjusted Pearson's covariation coefficient
1.0
0.5
0.0
-0.5
-1.0
CEN
IFT172
H
CEN
BB:
FP:

Figure 5

A

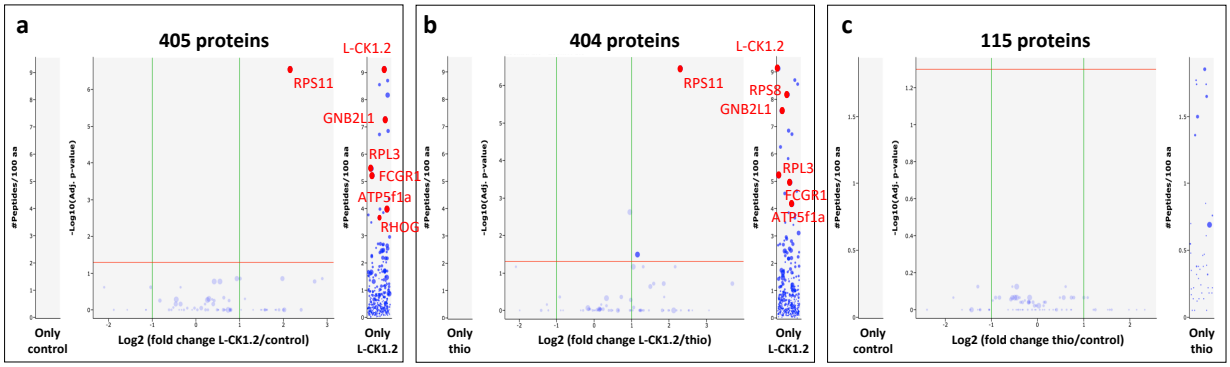
a
405 proteins
L-CK1.2
RPS11
GNB2L1
RPL3
FCGR1
ATP5f1a
RHOG
#Peptides/100 aa
-Log10(Adj. p-value)
Only control
Log2 (fold change L-CK1.2/control)
Only L-CK1.2
b
404 proteins
L-CK1.2
RPS11
RPS8
GNB2L1
RPL3
FCGR1
ATP5f1a
Only thio
Log2 (fold change L-CK1.2/thio)
Only L-CK1.2
c
115 proteins
Only control
Log2 (fold change thio/control)
Only thio

B

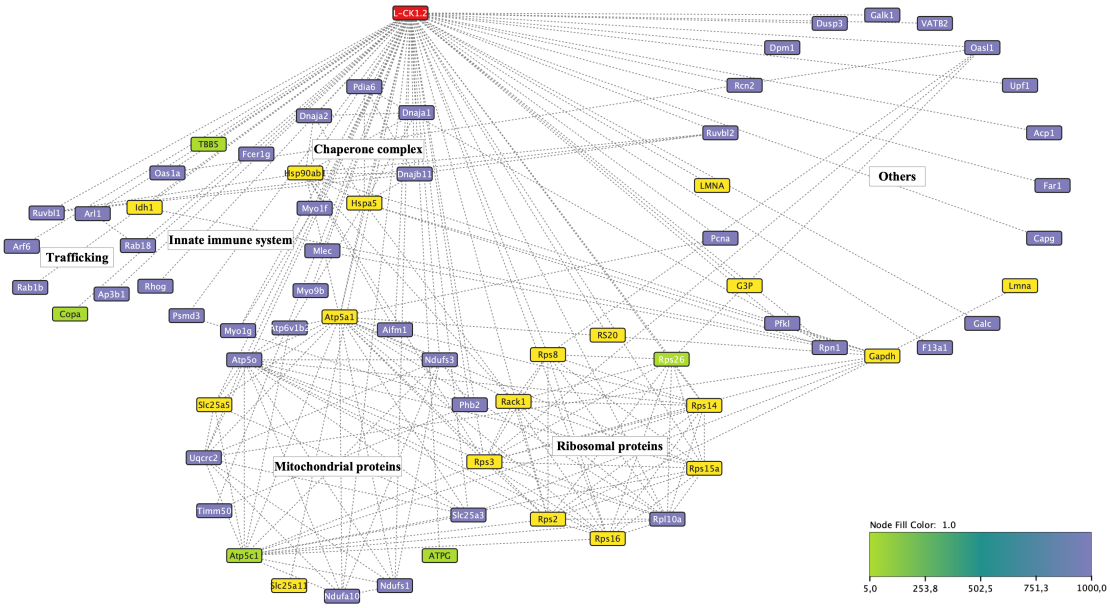
L-CK1.2
Chaperone complex
Innate immune system
Trafficking
Mitochondrial proteins
Ribosomal proteins
Others
Node Fill Color: 1.0
5,0
253,8
502,5
751,3
1000,0

C

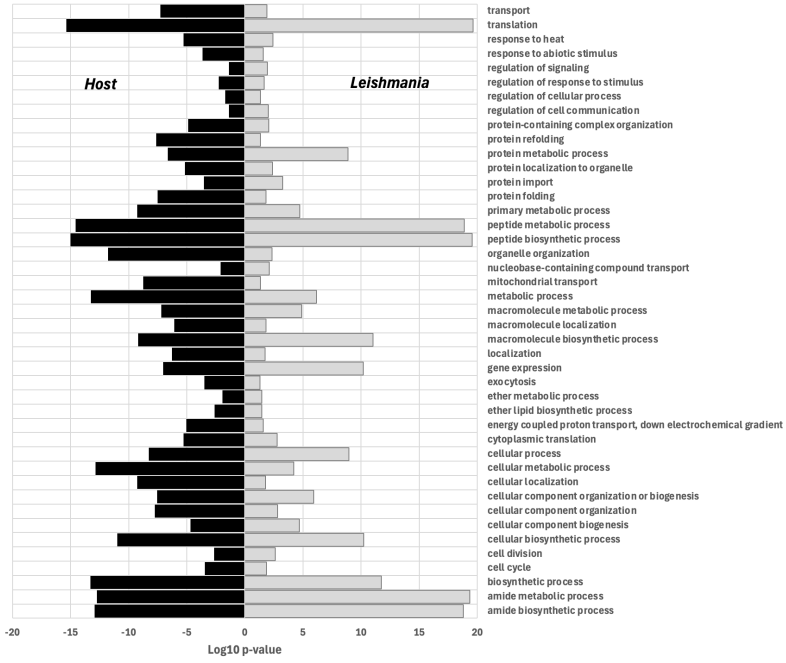
Host
Leishmania
transport
translation
response to heat
response to abiotic stimulus
regulation of signaling
regulation of response to stimulus
regulation of cellular process
regulation of cell communication
protein-containing complex organization
protein refolding
protein metabolic process
protein localization to organelle
protein import
protein folding
primary metabolic process
peptide metabolic process
peptide biosynthetic process
organelle organization
nucleobase-containing compound transport
mitochondrial transport
metabolic process
macromolecule metabolic process
macromolecule localization
macromolecule biosynthetic process
localization
gene expression
exocytosis
ether metabolic process
ether lipid biosynthetic process
energy coupled proton transport, down electrochemical gradient
cytoplasmic translation
cellular process
cellular metabolic process
cellular localization
cellular component organization or biogenesis
cellular component organization
cellular component biogenesis
cellular biosynthetic process
cell division
cell cycle
biosynthetic process
amide metabolic process
amide biosynthetic process
-20
-15
-10
-5
0
5
10
15
20
Log10 p-value